ROM SAF Report 41
Ref: SAF/ROM/DMI/REP/RSR/041
Web: www.romsaf.org
Date: 6 July 2021

EUMETSAT
ROM SAF
RADIO OCCULTATION METEOROLOGY

**ROM SAF Report 41**

# Assessment of sensitivity of the ROM SAF 1D-Var solutions to various error covariance choices

J. K. Nielsen

DMI, Copenhagen

### Document Author Table

| | ***Name*** | ***Function*** | ***Date*** |
|---|---|---|---|
| ***Prepared by:*** | Johannes K. Nielsen | ROM SAF Project Team | 6 July 2021 |
| ***Reviewed by:*** | Hans Gleisner | Climate Coordinator | 14 January 2021 |
| ***Reviewed by:*** | Sean Healy | Science Coordinator | 28 May 2021 |
| ***Approved by:*** | Kent B. Lauritsen | Project Manager | 6 July June 2021 |

### Document Change Record

| ***Issue/Revision*** | ***Date*** | ***By*** | ***Description*** |
|---|---|---|---|
| Version 0.1 | 24 December 2020 | JKN | Draft version for internal DMI review. |
| Version 0.2 | 14 January 2021 | JKN | Updated after review by H. Gleisner. |
| Version 0.3 | 21 June 2021 | JKN | Updated version following review of S. Healy. |
| Version 1.0 | 6 July 2021 | JKN | Final version |

### ROM SAF

The Radio Occultation Meteorology Satellite Application Facility (ROM SAF) is a decentralised processing centre under EUMETSAT which is responsible for operational processing of GRAS radio occultation (RO) data from the Metop and Metop-SG satellites and radio occultation data from other missions. The ROM SAF delivers bending angle, refractivity, temperature, pressure, humidity, and other geophysical variables in near real-time for NWP users, as well as reprocessed Climate Data Records (CDRs) and Interim Climate Data Records (ICDRs) for users requiring a higher degree of homogeneity of the RO data sets. The CDRs and ICDRs are further processed into globally gridded monthly-mean data for use in climate monitoring and climate science applications.

The ROM SAF also maintains the Radio Occultation Processing Package (ROPP) which contains software modules that aid users wishing to process, quality-control and assimilate radio occultation data from any radio occultation mission into NWP and other models.

The ROM SAF Leading Entity is the Danish Meteorological Institute (DMI), with Cooperating Entities: i) European Centre for Medium-Range Weather Forecasts (ECMWF) in Reading, United Kingdom, ii) Institut D'Estudis Espacials de Catalunya (IEEC) in Barcelona, Spain, and iii) Met Office in Exeter, United Kingdom. To get access to our products or to read more about the ROM SAF please go to: https://www.romsaf.org

### Intellectual Property Rights

**Abstract**

A series of experiments based on the ROM SAF Offline v1.1 processessing chain were performed to test the 1D-Var sensitivity to various choices of observation uncertainty and error correlation. The version of 1D-Var used as baseline was 1DV v4.2, the version used for production of ROM SAF Offline v1.1 data set. The test data set chosen was a series of Metop and COSMIC GNSS radio occultations, collocated with nighttime GRUAN RS92 radiosondes. Six perturbations of the refractivity error covariance matrix were probed, to test sensitivity to both uncertainty magnitude and correlation structure. Results were evaluated in terms of changes in bias, Desroziers diagnostics and averaging kernels, broken down on mission and latitude bands.

Generally 1D-Var temperature is negatively biased in the troposphere and positively biased in the stratosphere. 1D-Var specific humidity is dry biased in most of the troposphere. Deflation of the refractivity error covariance enhances these biases. Suppression of refractivity error correlations also increases 1D-Var temperature bias structures in stratosphere, but has little effect on tropospheric temperature retrievals. The negative specific humidity bias in middle and upper troposphere is enhanced by suppression of refractivity error correlations. Desroziers diagnostics suggests that a substantial deflation of tropospheric refractivity error covariance, with a factor of 2 or 3, can be justified.

By comparing Desroziers estimates of refractivity variance, with assumed variance, and relate that to the analytical expression for Desroziers matrices it can be inferred that the current ROM SAF background uncertainties are overestimated.

# Contents

# 1 Introduction

In the ROM SAF processing chains tropospheric parameters (temperature, specific humidity and surface pressure) are retrieved from GNSS Radio Occultation (RO) profiles with a 1D-Var algorithm. 1D-Var is commonly used to estimate atmospheric parameters from RO observations [7]. The particular 1D-Var implementation used in the ROM SAF is documented in the ATBD [8]. The performance of — and results from — the 1D-Var implementation are crucially dependent on the assumed uncertainties, specified as error covariance matrices for background profiles $\mathbf{B}$ and refractivity $\mathbf{R}$ (see [8]). The operational $\mathbf{B}$ is calculated from ERA-Interim error of first guess, and the operational $\mathbf{R}$ is a parameterized error estimate roughly in accordance with estimates in [11] and [6].

The results presented in this report are related to the ROM SAF CDOP-3 Work Package 2330 [3] on assessing the sensitivity of the 1D-Var results to error covariance choices. This is investigated by characterizing the impact of variations of refractivity error covariance matrices on the current offline ROM SAF 1D-Var performance. Sensitivity to refractivity error covariance is assessed through experiments where the 1D-Var configuration is left untouched, except for the refractivity error covariance matrix $\mathbf{R}$, of which different properties are substantially — but not radically — perturbed. The conclusions of WP 2330 is presented in this report.

As mentioned, the refractivity error covariance is only one of the inputs determining the performance of 1D-Var, so this report only includes one aspect of the 1D-Var sensitivity to input. The disentanglement of temperature and humidity signal in RO 1D-Var is determined by the background profile and the background error covariance matrix $\mathbf{B}$. The impact of perturbation of $\mathbf{R}$ is primarily to change the weighting between observation and background information in the retrieval. But indirectly, through correlation patterns, variations of $\mathbf{R}$ can be expected to also impact the weighting between dry and wet contribution to the refractivity in the 1D-Var solution.

For this study data from Metop A and B and COSMIC-1 are processed with all the used $\mathbf{R}$-matrices. In order to reference the performance to an independent data source, the test data is chosen as a subset of radio occultations collocated with RS92 radiosondes from the GCOS Reference Upper-Air Network (GRUAN) [2].

The following experiments are performed:

1. The baseline run is performed with the configuration used for ROM SAF Offline and corresponding $\mathbf{R}$-matrix. See section 3.1.
2. Simple deflation: $\mathbf{R} \rightarrow \mathbf{R}/4$
3. Simple inflation: $\mathbf{R} \rightarrow 4\mathbf{R}$
4. Correlation length scaling: $\mathbf{R}$ correlation length divided by 5.
5. Troposphere focus: A combination of deflation, scaling with the additional feature that parameterization, STDV = 0.1% of refractivity, is extended below the tropopause, to 3 km.
6. ECMWF operational: The bending angle covariance used operationally at ECMWF, mapped to refractivity space.
7. ECMWF, min 1 $\mu$rad: The ECMWF observation error covariance, with the lower limit bending angle uncertainty changed from 3 $\mu$rad (operational) to 1 $\mu$rad.

The next chapter (2) describes the data, the processing and the analysis in a little more detail. The

main part of the report, chapter 3, is structured as 7 sections, all starting with a brief statement of the experiment. The results are presented separately in three subsections representing high, mid and low latitudes. Each latitude section is separated into “diagnostics” (Desroziers and Averaging Kernels) and “performance” results (changes in solution biases). The performance is shown separately for Metop and COSMIC. This is chosen deliberately to catch possible spurious features caused by single or few outliers in the data set. In Chapter 4 the dependency of Desroziers estimates on 1D-Var configuration is analyzed. Chapter 5 contains a summary of the results with a few conclusions.

## 2 Data and method

The experiments are designed to test the ROM SAF 1D-Var sensitivity to choices of observation uncertainty and uncertainty correlation. The occultations are chosen such that they are collocated with GRUAN RS92 [2] sondes, in the period between 2006 and 2016. The dataset contains 8607 COSMIC collocations, 6444 Metop A and B collocations. The background profiles used for 1D-Var are interpolated from ERA5 forecasts as described for offline processing in [8].

The 1D-Var algorithm used for all the following results is described in [8], and will not will not be described in further detailed here.[1]

For each experiment Desroziers diagnostics ([1] and [5, 9]) are applied, by estimation of the matrix

$$\tilde{\mathbf{R}} = \overline{(\text{observation} - \text{background})(\text{observation} - \text{solution})^T} \tag{2.1}$$

in refractivity space. This matrix would approach the assumed $\mathbf{R}$ with an ideal well tuned 1D-Var. Here $\tilde{\mathbf{R}}$ is examined to indicate to which degree $\mathbf{R}$ is chosen correctly. $\tilde{\mathbf{R}}$ is not an estimate of a "true" error covariance, since it dependents on both the data and $\mathbf{B}$ and $\mathbf{R}$ itself. Desroziers diagnostics can be regarded as a consistency check.

Another diagnostic tool is averaging kernels ($\mathbf{KH}$) [4],

$$\mathbf{KH} = (\mathbf{H^T R^{-1} H} + \mathbf{B^{-1}})^{-1} \mathbf{H^T R^{-1} H}, \tag{2.2}$$

$\mathbf{H}$ being the linearized forward model. The averaging kernels measure the solutions atmospheric parameters sensitivity to virtual perturbations in the atmospheric parameters themselves. For each experiment a few examples of averaging kernels are presented. If $\mathbf{KH}$ was a unit delta function at some level, it would mean that a perturbation of the state vector at that level would map, one to one, into that level in the 1D-Var solution.

Retrieved temperature, specific humidity and pressure are compared to background profiles. GRUAN collocated profiles are also analyzed for all occultations. Only nighttime GRUAN RS92 profiles are used, to avoid solar heating bias. The GRUAN systematic temperature uncertainty is in the order of 0.1 K (tropsphere) 0.2 K (stratosphere). The GRUAN systematic humidity uncertainty is in the order of 5-10%. The GRUAN combined pressure uncertainty is in the order of 0.6-0.2 hPa.

All results are compared on ERA5 model levels, with ERA5 forecast as reference, and plotted with geopotential height as free variable. GRUAN data are interpolated to ERA5 model levels.

The refractivity profiles used in the 1D-Var algorithm were taken from the ROM SAF CDR v1.0, and the QC from that dataset is inherited. In addition the success of the 1D-Var is required, implying an additional check on the cost function ($2J/m < 5$) and number of iterations (to be kept under 25).

[1] The Offline v1.1 offline chain has a bug, preventing the forward model to correctly represent 1D-Var solutions with specific humidity below zero. In the experiments represented here, the bug has been fixed such that $q$ is mapped linearly into refractivity space, and solutions where the humidity falls below zero due to noise are allowed.

# 3 Results

The results are presented in 7 sections with a few specific comments addressed to each experiment in the beginning of the experiment's section. The first section is devoted to the baseline run, which also introduces the diagnostic (Desroziers and averaging kernel) plots. In the remaining six sections mean values, compared to ERA5 forecast, are shown along with the baseline and GRUAN data. The word "bias" is used a little sloppy in this context; meaning deviation from ERA5. One thing to bare in mind is that the GRUAN collocations are very sparse in the tropics, meaning that there is a high uncertainty on both bias and covariance estimates. In the Desroziers estimated matrices this is seen as increased apparent fine scale structure in the tropical results, which must be dismissed as noise.

## 3.1 Baseline experiment

The baseline dataset is produced with the operational dynamic tropopause dependent refractivity error covariance assumption described in [8]. In brief the baseline covariance matrix is defined such that the standard deviation (square root of diagonal of $\mathbf{R}$) is 0.2% of the refractivity above the tropopause, increasing lineary to 2% at the surface. In the top of the profiles the refractivity standard deviation is constrained such that it never falls below 0.02 N-Units. At all altitudes an exponential refractivity correlation function with 3km decay length is assumed.

There are a few things to note about the baseline Desroziers matrices (shown in Figures 3.1, 3.2 and 3.3): The standard deviation found in the troposphere, at all latitudes for both Metop and COSMIC is much smaller than the assumed standard deviation $\mathbf{R}$. This is also the case in the upper stratosphere, especially at polar and mid latitudes. The Desroziers matrices are not symmetric in general. The lower and mid stratosphere refractivty errors are anticorrelated with the troposphere. These features will show to be quite prominent for all experiments. The Desroziers matrix seems to have longer correlation length that the original $\mathbf{R}$ everywhere, except for a small interval at the crossover between correlated and anticorrelated refractivity error around 20 km.

It should be noted that in terms of covariance (rather than correlation) the difference between assumed and estimated off-diagonal terms is smaller. The enhanced Desroziers correlation lengths are associated with altitudes where the standard deviation (diagonal) is reduced in the Desroziers matrix, and consequently the off diagonal elements are *relatively* large. Since the correlation matrix is normalized with the diagonal elements of the covariance matrix, reduced standard deviation leads to enhanced correlations at a given level.

The averaging kernels reflects that there is not much humidity sensitivity in upper and lower troposphere in the baseline run.

In the next section (Section 3.2), in Figures 3.5, 3.7 and 3.9, the biases of the baseline are plotted with blue color along with GRUAN (green color) as references for high, mid and low latitudes. This convention is kept for similar figures in all the following sections. The baseline and GRUAN mean values are almost unchanged for all runs, only differing slightly due to small differences in QC.

Generally the baseline 1D-Var systematic temperature difference to GRUAN lies below 0.3 K. Between 15 and 30 km the baseline tends to be drawn away from the background towards the positively biased GRUAN temperature. For humidity the baseline and GRUAN agrees within the GRUAN systematic uncertainty (5%) up to 6 km (8km for mid-latitudes). The GRUAN pressure has a strong

positive bias in the stratosphere, suggesting that there may be some bias in geopotential height calculations, leading to false altitude attribution of temperature in the stratosphere.

Generally the baseline specific humidity is dry biased in the lower troposphere, when compared to the background (ERA5 forecast). At mid latitudes the baseline bias goes down to -0.2 g/kg and GRUAN is wet biased up to at least 0.1 g/kg. There is noticeable difference between GRUAN bias of Metop and COSMIC at 2 km. Except for that discrepancy, Metop and COSMIC performs quite similarly. Between 4 and 7 km the baseline is slightly dry (2-3%) for high and mid-latitudes. GRUAN humidity is not to be trusted above the tropopause and GRUAN temperatures are not to be trusted above 40 km. At high latitudes the baseline temperature is generally negatively biased (-0.1K), compared to the ERA5 background at low altitude. This is a 1D-Var artifact, not to be resolved here. At mid-latitudes the baseline shows a negative temperature bias (0.1-0.2 K) at the tropopause, accompanied with similar drop in GRUAN temperature. This drop is attributed to superior vertical resolution of GRUAN and RO at the tropopause.

There are only around 100 tropical night collocations for each mission, so the tropical comparisons will not be interpreted too much. However, it can be inferred that in terms of mid troposphere humidity the baseline and GRUAN agrees in the same way as for midlatitudes, except that the agreement reaches up to 10 km. In the lowest tropical troposphere GRUAN specific humidity departs up 0.7 to 0.8 g/kg, and GRUAN temperature departs quite dramatic with a systematic structure for both satellite missions. Note that most of these profiles come from one station in Singapore.

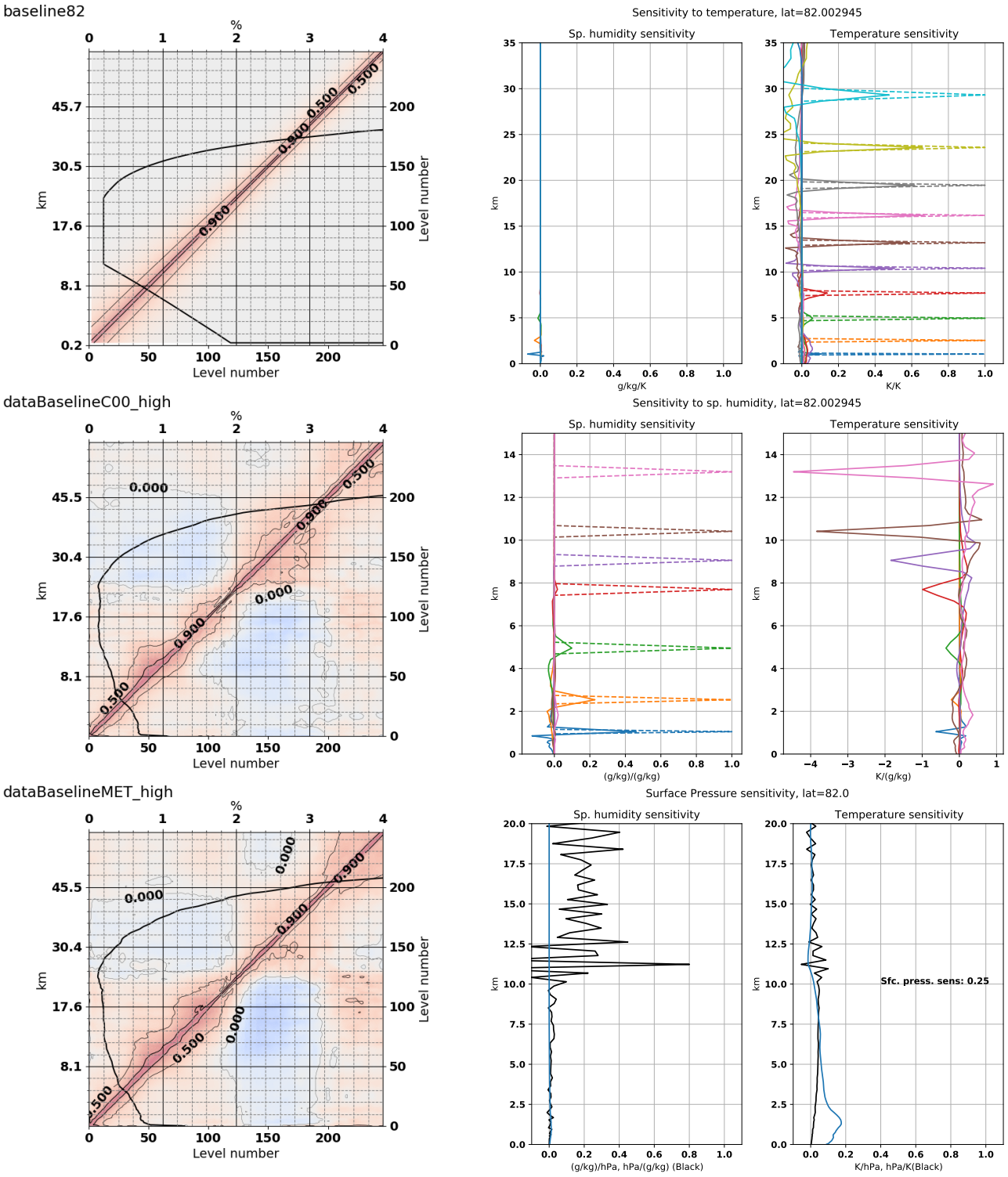


**Figure 3.1: Baseline high latitudes. Left:** Refractivity error covariance matrices illustrated as contour plots of the correlation matrix, with superimposed relative standard deviation plotted as percentage vertically (axis on top). Top: An example of high latitude $\mathbf{R}$ used as input operationally. Middle: Derived Desroziers $\mathbf{R}$ from 1D-var performed on COSMIC. Bottom: Derived Desroziers $\mathbf{R}$ from 1D-var performed on Metop. **Right:** Averaging kernels derived for baseline configuration. The averaging kernel plots also shows the virtual perturbation (dashed lines) that would lead to the given averaging kernel response. The figures are shown in pairs. Top: Sp. Humidity and temperature response to temperature perturbation. Middle: Specific humidity and temperature response to specific humidity perturbation. Bottom: Specific humidity and temperature response to 1 hPa pressure perturbation (blue) and pressure response to specific humidity and temperature perturbation (black). Also shown as number: pressure response to pressure perturbation.

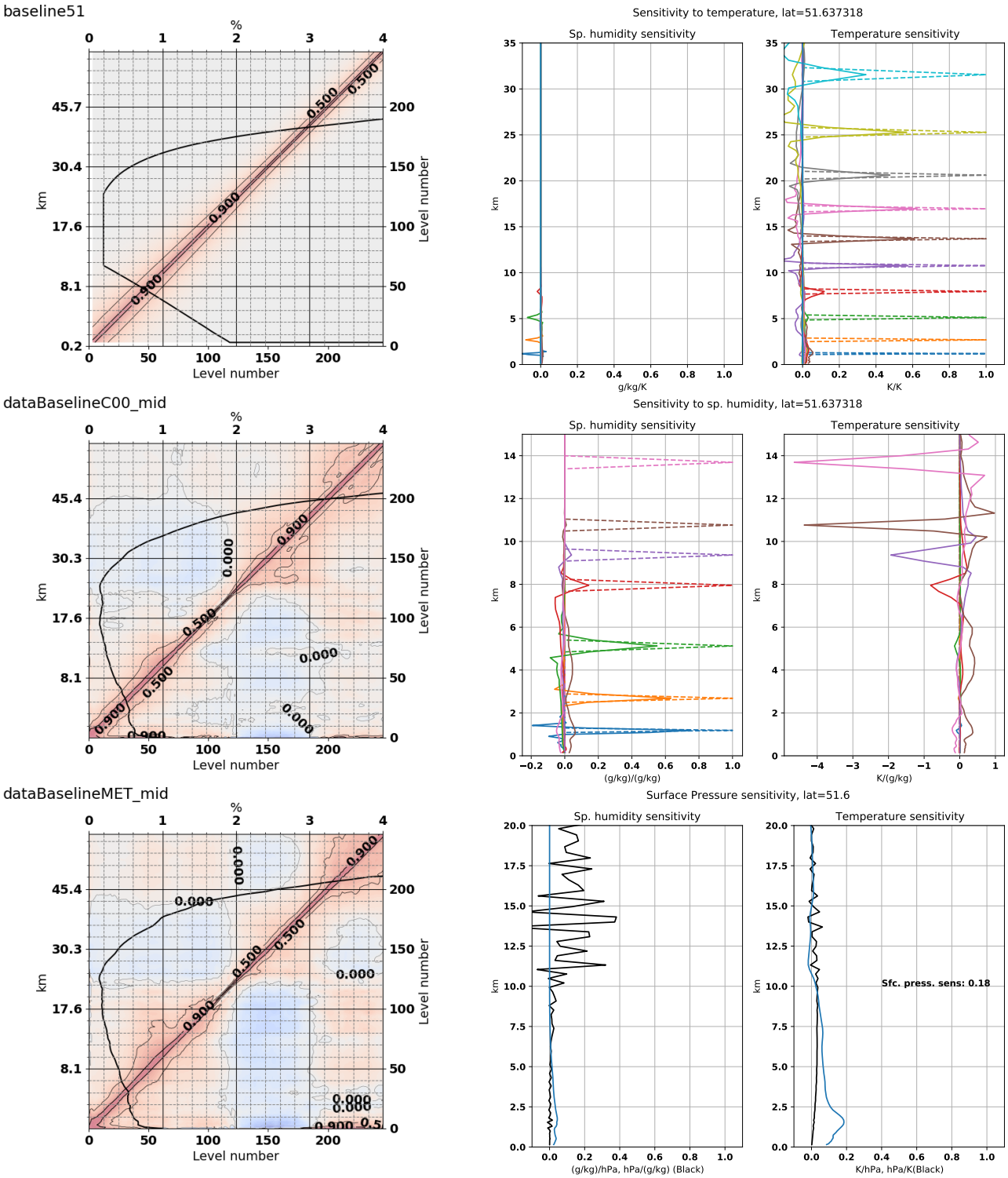


**Figure 3.2: Baseline mid latitudes. Left:** Refractivity covariances, as in Fig. 3.1, with $30 < |lat| < 60$ degrees. Top: An example of high latitude $\mathbf{R}$ used as input operationally. Middle: Derived Desroziers $\mathbf{R}$ from 1D-var performed on COSMIC. Bottom: Derived Desroziers $\mathbf{R}$ from 1D-var performed on Metop. **Right:** Example of averaging kernels. As in Fig. 3.1, with $30 < |lat| < 60$ degrees.

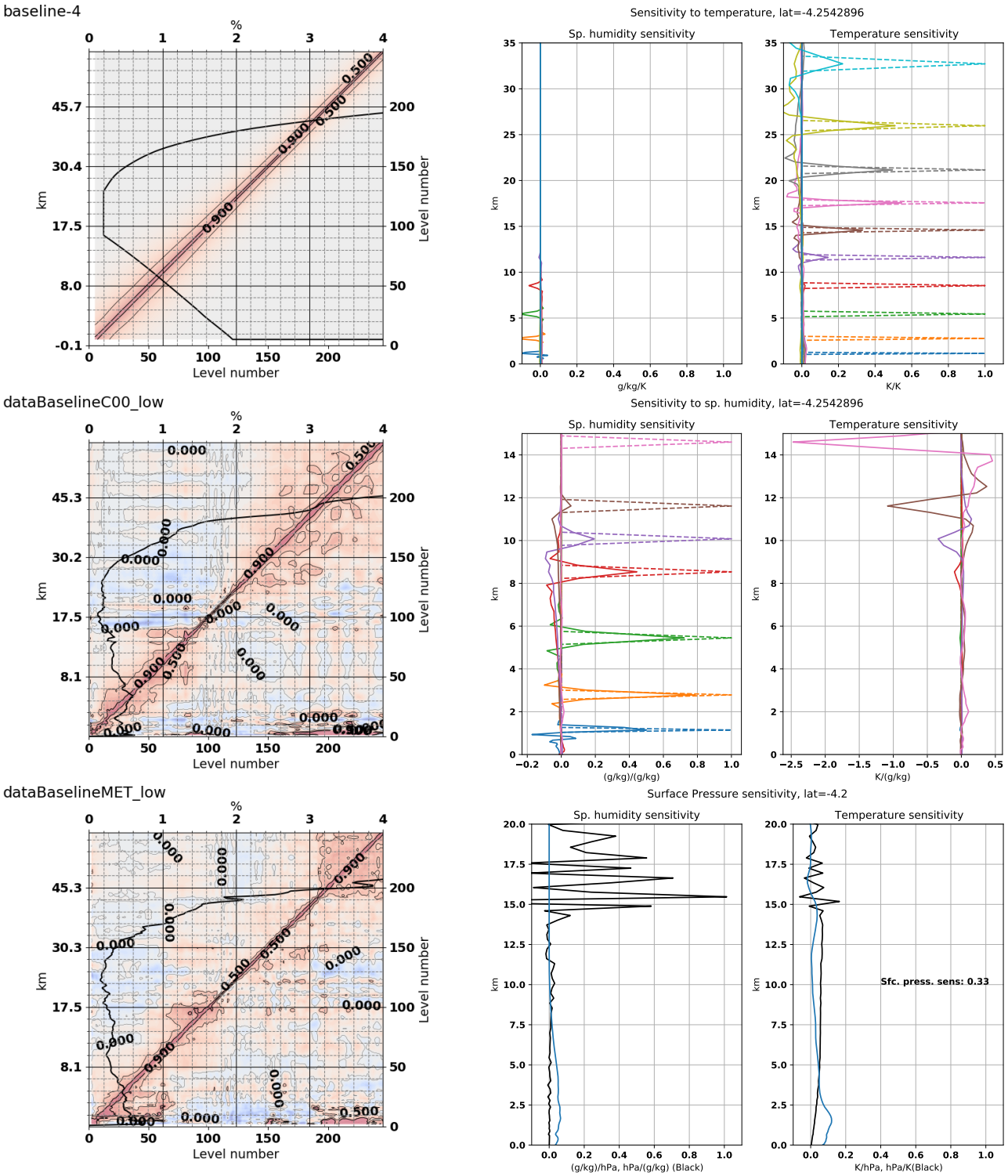


**Figure 3.3: Baseline low latitudes. Left:** Refractivity covariances, as in Fig. 3.1, with $|lat| < 30$ degrees. Top: An example of high latitude $\mathbf{R}$ used as input operationally. Middle: Derived Desroziers $\mathbf{R}$ from 1D-var performed on COSMIC. Bottom: Derived Desroziers $\mathbf{R}$ from 1D-var performed on Metop. **Right:** example of averaging kernels. As in Fig. 3.1, with $|lat| < 30$ degrees.

## 3.2 Operational R-matrix deflation

The deflation experiment is performed by simply putting the refractivity standard deviation to one half of the operational STDV, and then rerun 1D-Var. The inflated error covariance matrices, show in upper left corners of Figures 3.4, 3.6 and 3.8 have a small drop near the surface, due to an upper refractivity uncertainty limit of 10 N-units in the ROPP code. Remarkably the Desroziers $\tilde{\mathbf{R}}$ matrix seems to just follow the suggested $\mathbf{R}$, except for the troposphere and upper stratosphere, where the diagonal of $\tilde{\mathbf{R}}$ is even smaller than the deflated diagonal of $\mathbf{R}$. The correlations appears unchanged. As expected the sensitivity is increased, which is seen in the averaging kernels shown in the right columns of Figures 3.4, 3.6 and 3.8. For instance humidity sensitivity at 8 km goes from close to 0.1 (baseline), to well above 0.2. In the tropics sensitivity of 0.1 is obtained above 11.5 km. Looking at mean values, Figures. 3.5 and 3.7 and 3.9, the tropospheric dry bias is enhanced slightly, resulting in an even larger deviation from GRUAN specific humidity in the lower troposphere. Generally the bias structure seen in the baseline run is enhanced, which is seen very clearly between 5-7 km (up to 10 km at mid latitudes). For both high and mid-latitudes the 1D-Var is pulling towards a lower humidity than ERA5 everywhere, except for the altitude range between 3 and 5 km, where RO and ERA5 agree, but GRUAN is positively biased.

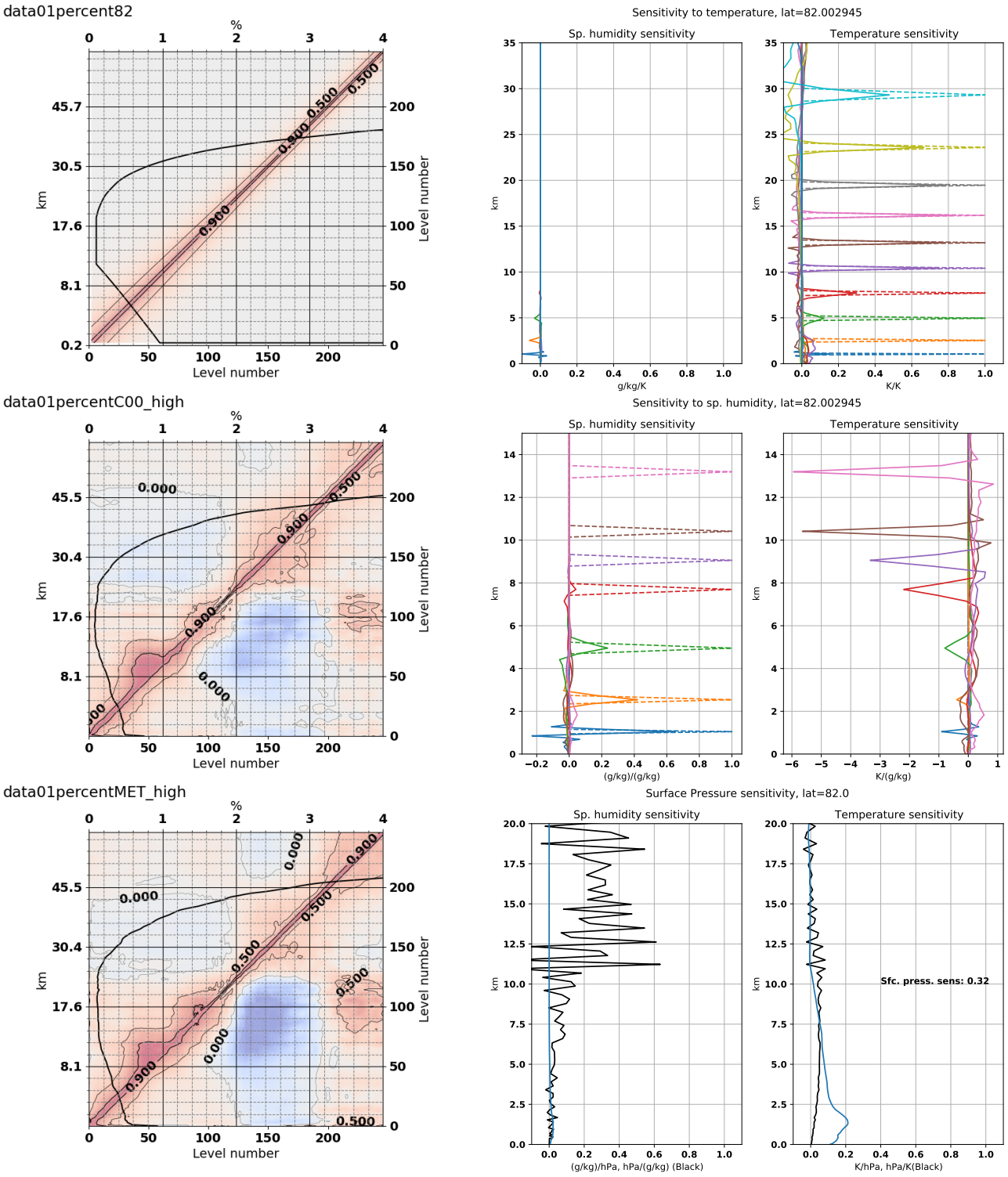


**Figure 3.4: Operational R-matrix deflation, diagnostics at high latitudes**. **Left:** Error covariances, as in Fig. 3.1 for $|lat| > 60$ degrees. **Right:** Averaging kernels, as in Fig. 3.1, for $|lat| > 60$ degrees.

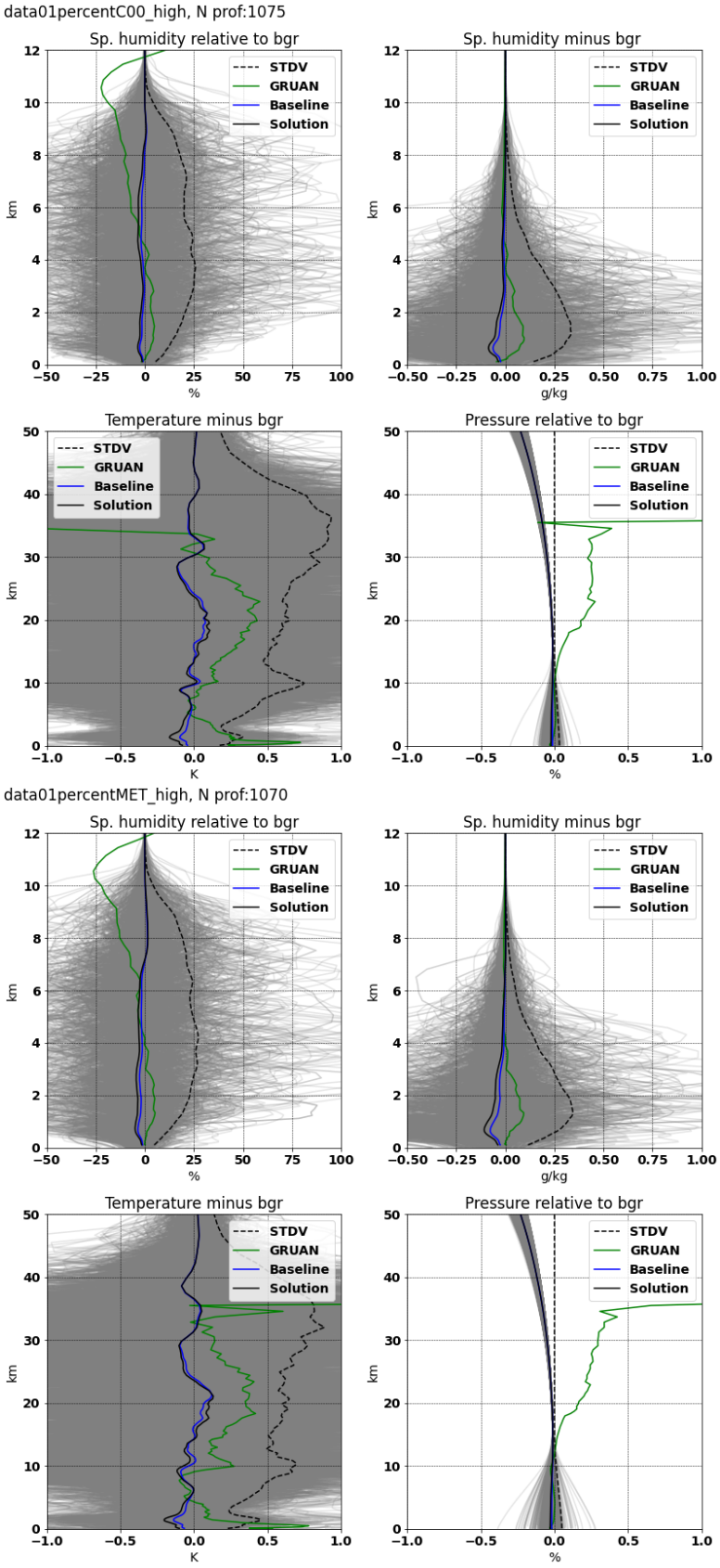


**Figure 3.5: Operational R-matrix deflation, |lat|>60 degrees**. 1D-Var results (humidity, temperature and pressure, with background subtracted). Top: COSMIC. Bottom: Metop. Gray curves show solution, black: mean solution, blue: baseline, green: GRUAN and dashed: solution minus background STDV.

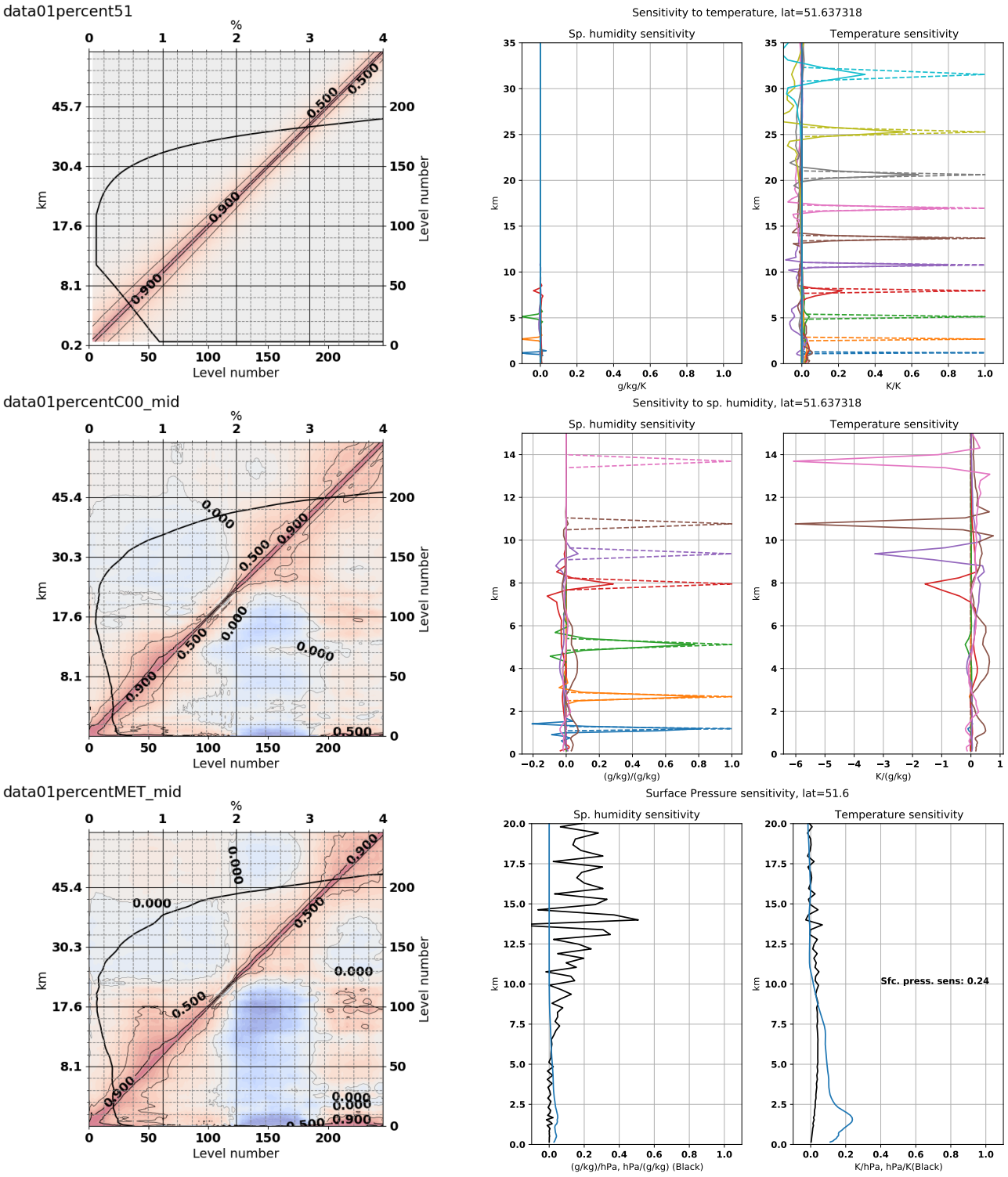


**Figure 3.6: Operational R-matrix deflation, diagnostics at mid latitudes**. **Left:** Error covariances, as in Fig. 3.1 for $30 < |lat| < 60$ degrees. **Right:** Averaging kernels, as in Fig. 3.1, with $30 < |lat| < 60$ degrees.

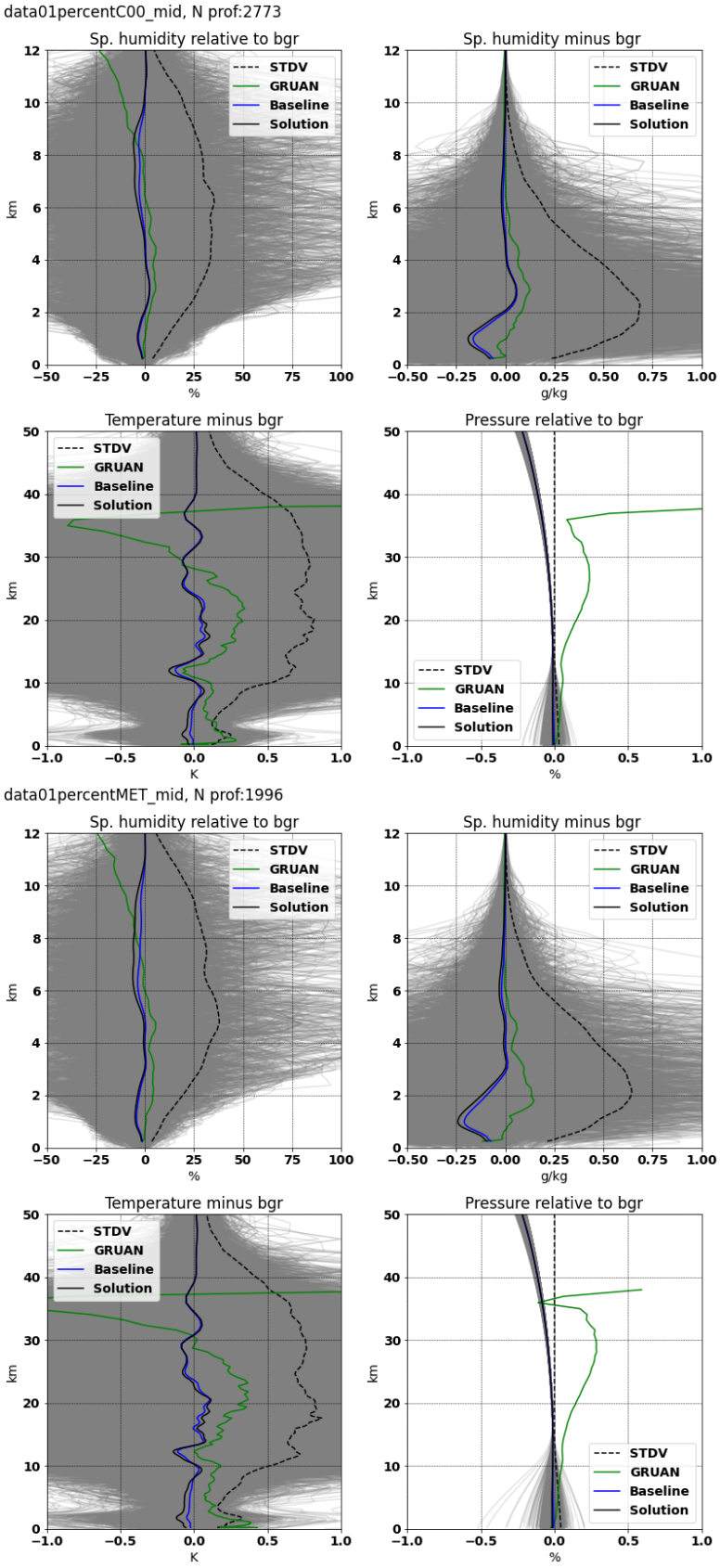


**Figure 3.7: Operational R-matrix deflation, 30<|lat|<60 degrees**. 1D-Var results (humidity, temperature and pressure, with background subtracted) degrees. Top: COSMIC. Bottom: Metop. Gray curves show solution, black: mean solution, blue: baseline, green: GRUAN and dashed: solution minus background STDV.

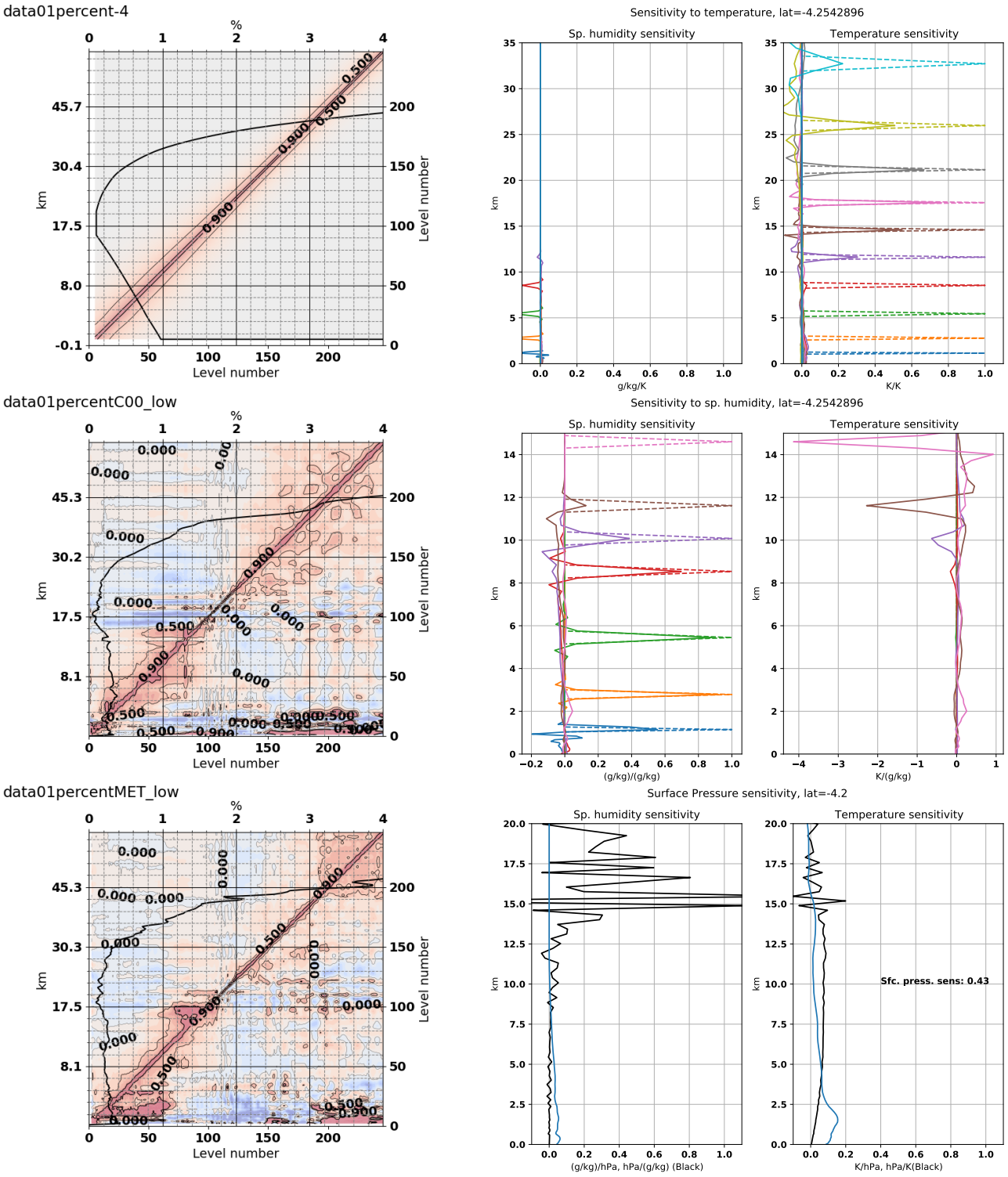


**Figure 3.8: Operational R-matrix deflation, diagnostics at low latitudes**. **Left:** Error covariances, as in Fig. 3.1 for $|lat| < 30$ degrees. **Right:** Averaging kernels, as in Fig. 3.1, with $|lat| < 30$ degrees.

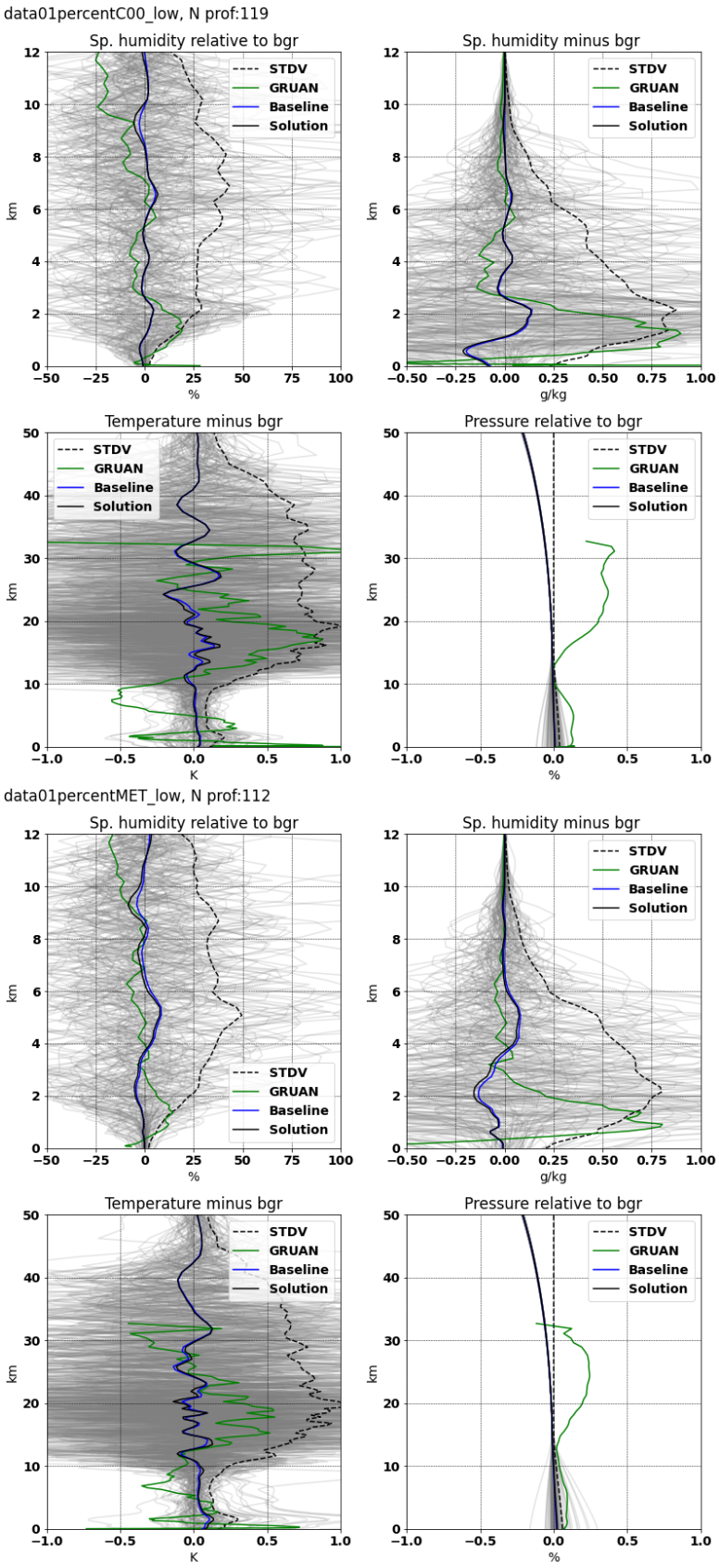


**Figure 3.9: Operational R-matrix deflation, |lat|<30 degrees**. 1D-Var results (humidity, temperature and pressure, with background subtracted). Top: COSMIC. Bottom: Metop. Gray curves show solution, black: mean solution, blue: baseline, green: GRUAN and dashed: solution minus background STDV.

### 3.3 Operational R-matrix inflation

The inflation is simply performed by setting the refractivity standard deviation to twice the operational STDV. Unlike in the deflation experiment the resulting Desroziers matrices (Figures 3.10,3.12 and 3.14) are not just following the "suggested" standard deviation of $\mathbf{R}$. At mid and high latitudes, the Desroziers standard deviation in the stratosphere remains more or less on the same magnitude as in $\mathbf{R}$ while in the tropics it tends do increase for both Metop and COSMIC. Generally the averaging kernels in figures 3.10,3.12 and 3.14 are a bit reduced, compared to the baseline. As one might expect the impact on mean values in Figures 3.11, 3.13 and 3.15 is the reverse of the impact of deflation, i.e. the solution moves closer to the background.

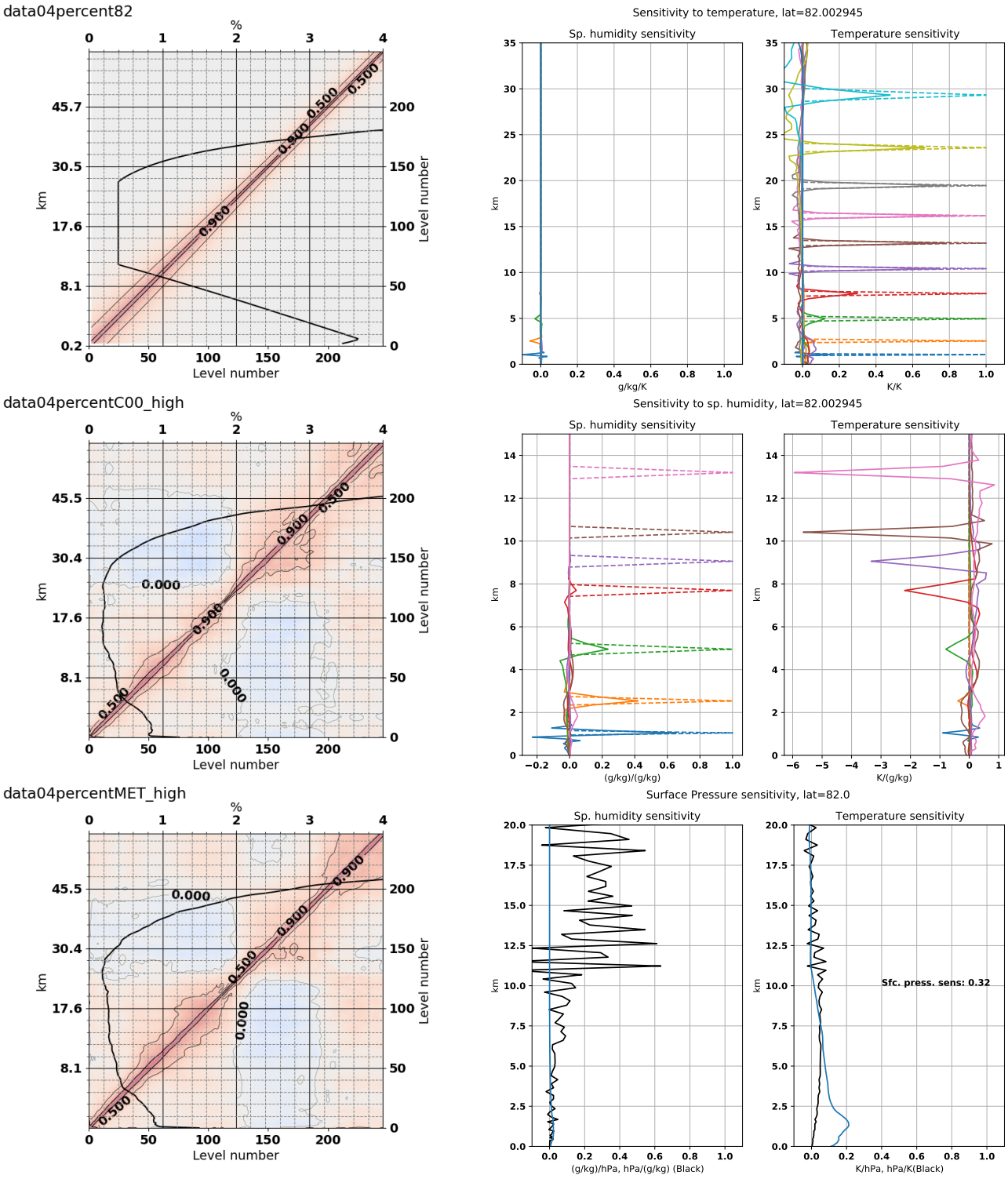


**Figure 3.10: Operational R-matrix inflation, diagnostics at high latitudes**. **Left:** Error covariances, as in Fig. 3.1 for $|lat| > 60$ degrees. **Right:** Averaging kernels, as in Fig. 3.1, for $|lat| > 60$ degrees.

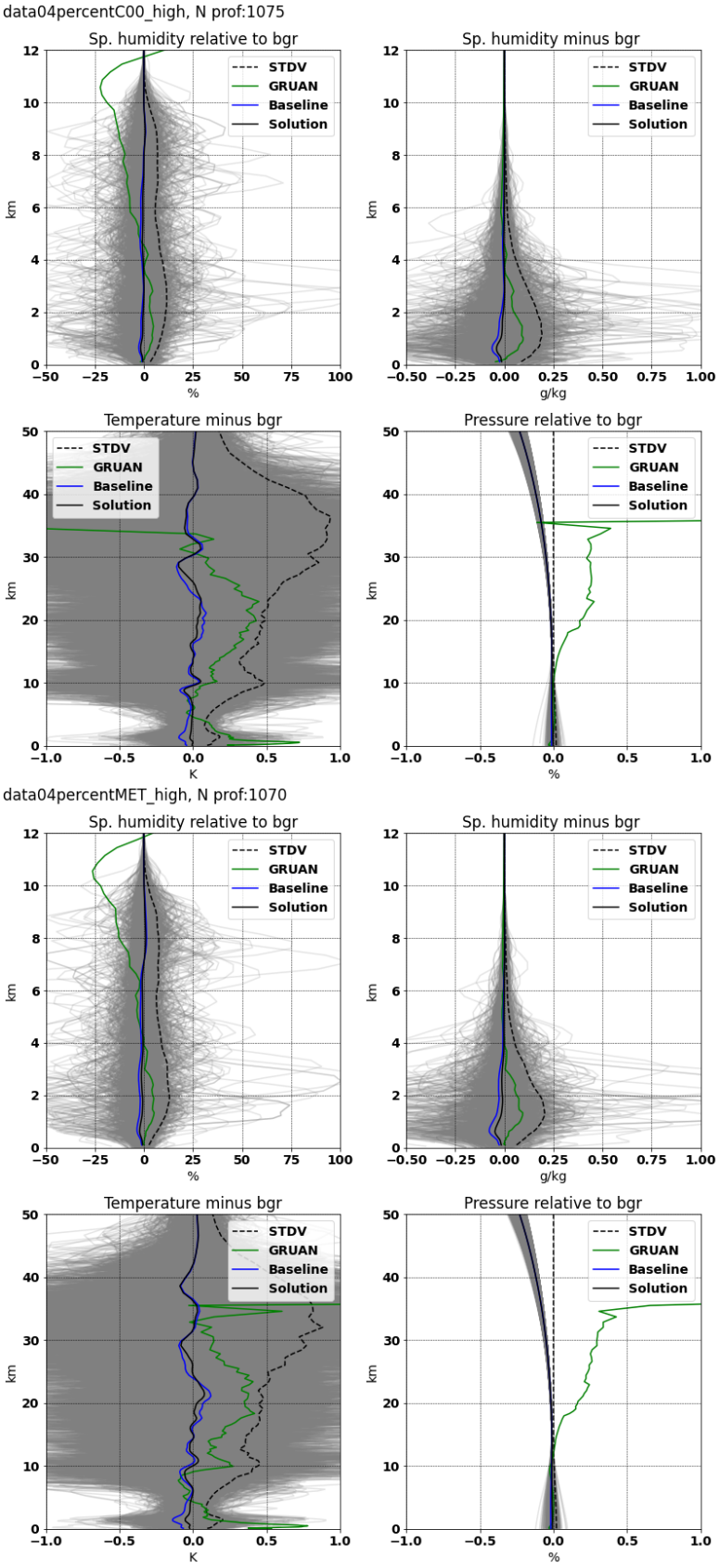


**Figure 3.11: Operational R-matrix inflation, |lat|>60 degrees**. 1D-Var results (humidity, temperature and pressure, with background subtracted). Top: COSMIC. Bottom: Metop. Gray curves show solution, black: mean solution, blue: baseline, green: GRUAN and dashed: solution minus background STDV.

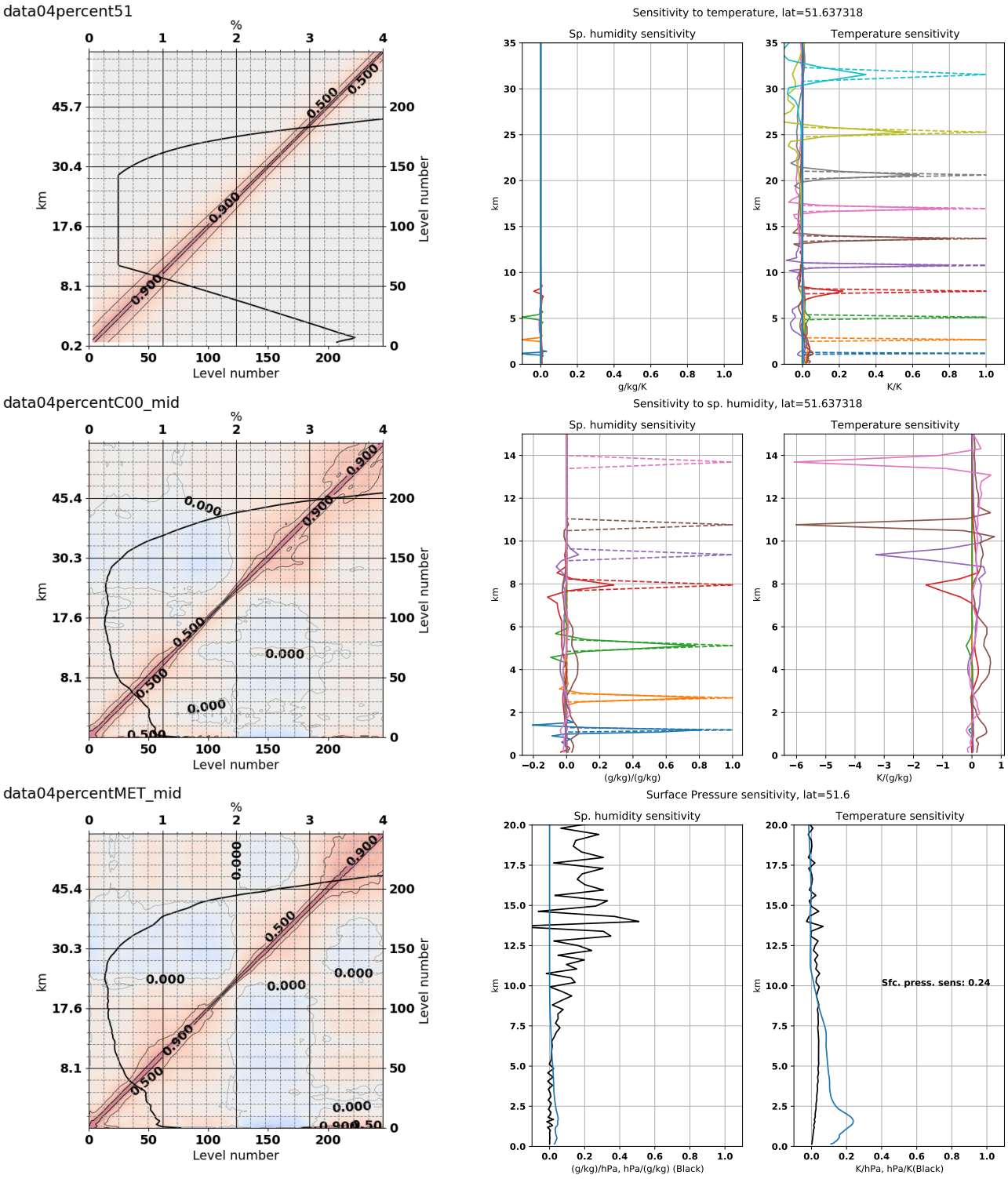


**Figure 3.12: Operational R-matrix inflation, diagnostics at mid latitudes**. **Left:** Error covariances, as in Fig. 3.1 for $30 < |lat| < 60$ degrees. **Right:** Averaging kernels, as in Fig. 3.1, with $30 < |lat| < 60$ degrees.

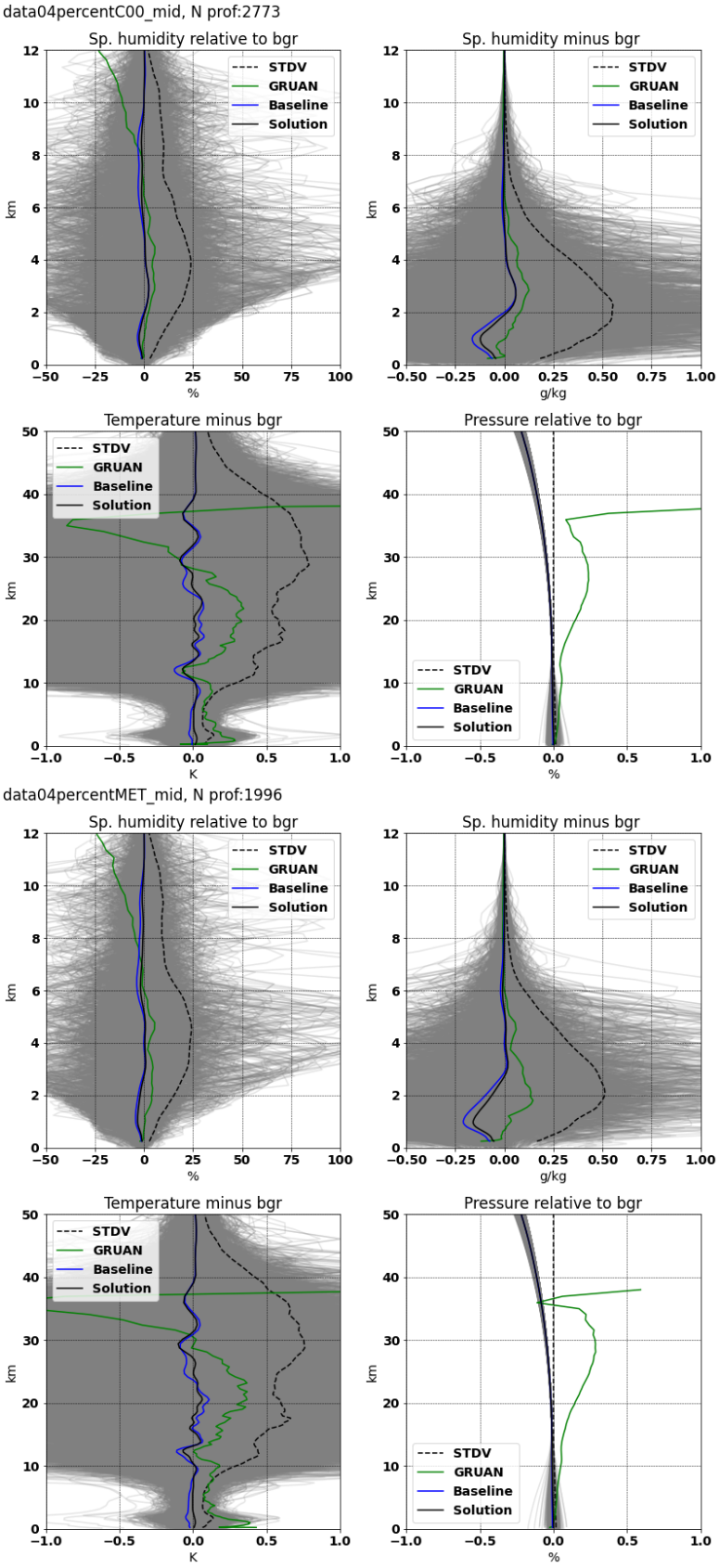


**Figure 3.13: Operational R-matrix inflation, 30<|lat|<60 degrees**. 1D-Var results (humidity, temperature and pressure, with background subtracted) degrees. Top: COSMIC. Bottom: Metop. Gray curves show solution, black: mean solution, blue: baseline, green: GRUAN and dashed: solution minus background STDV.

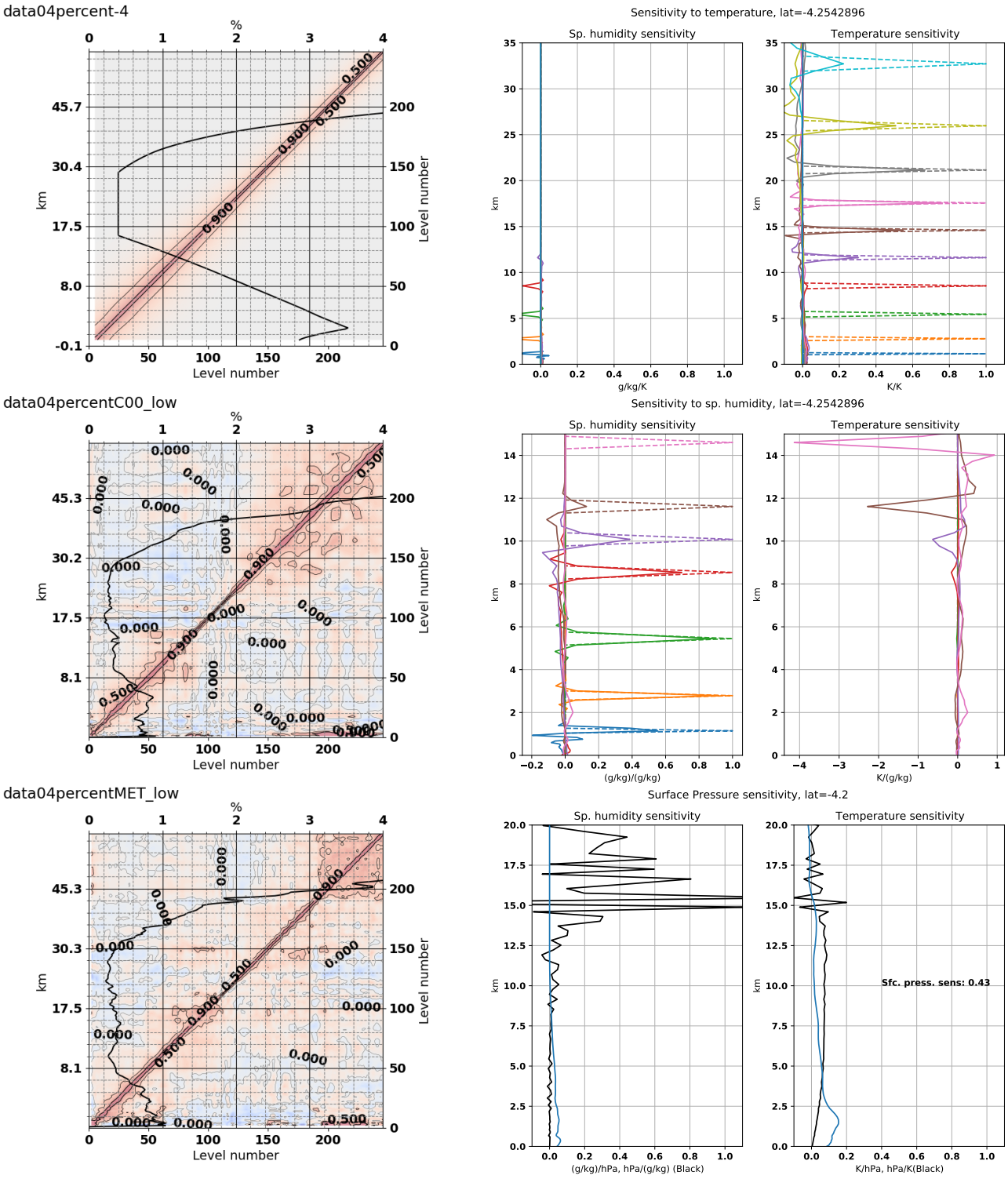


**Figure 3.14: Operational R-matrix inflation, diagnostics at low latitudes**. **Left:** Error covariances, as in Fig. 3.1 for $|lat| < 30$ degrees. **Right:** Averaging kernels, as in Fig. 3.1, with $|lat| < 30$ degrees.

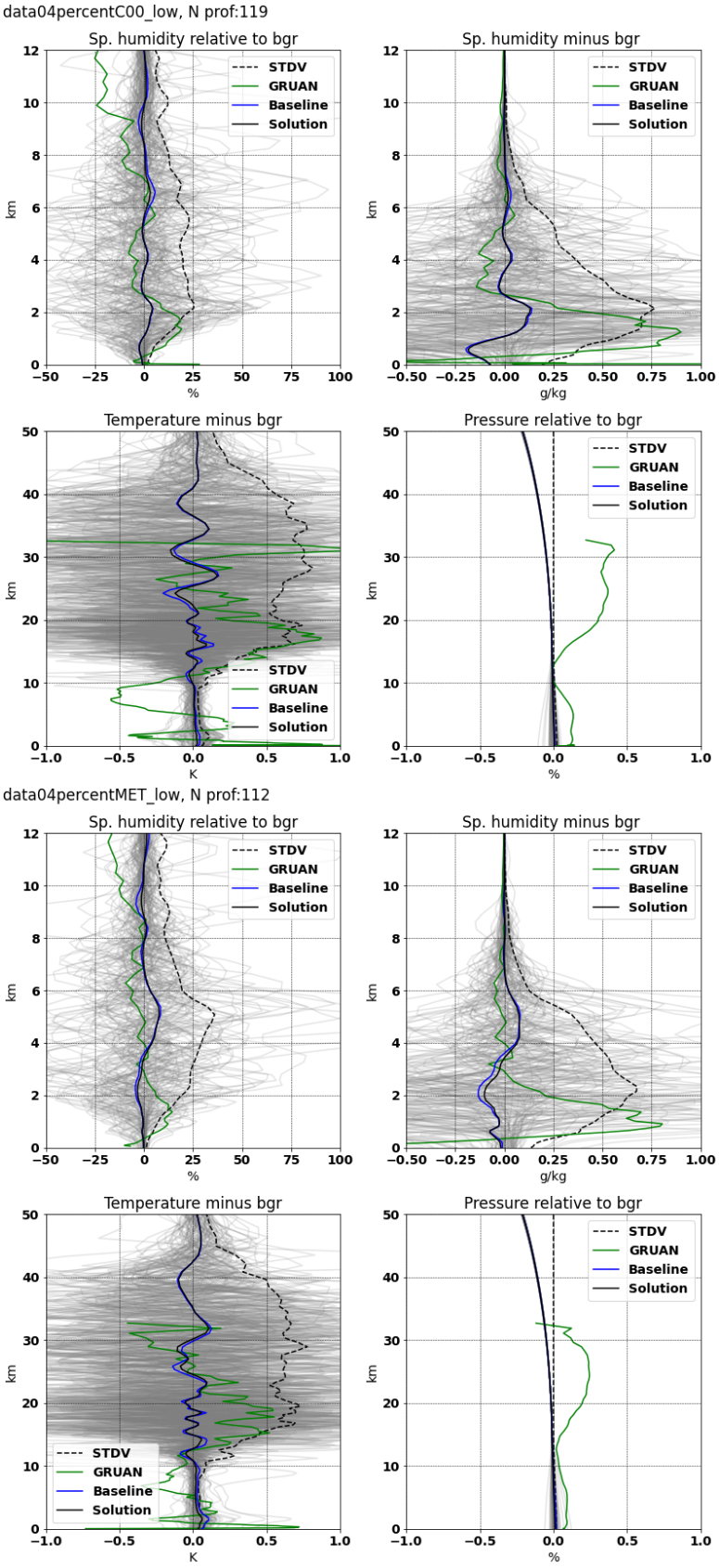


**Figure 3.15: Operational R-matrix inflation, |lat|<30 degrees**. 1D-Var results (humidity, temperature and pressure, with background subtracted). Top: COSMIC. Bottom: Metop. Gray curves show solution, black: mean solution, blue: baseline, green: GRUAN and dashed: solution minus background STDV.

### 3.4 Operational R-matrix with reduced correlation length

The reduced correlation length experiment is performed by changing the correlation length of the exponential refractivity error correlation function from the operationally used 3000 m to 600 m, in the calculation of the refractivity error covariance matrix. The resulting Desroziers covariance still has a lower standard deviation than the baseline $\mathbf{R}$ at all altitudes (Figures 3.16,3.18 and 3.20), and at the same time the correlations seems to have been slightly reduced, compared to the baseline Desroziers matrix. However the long range weak correlations pattern does not disappear in $\tilde{\mathbf{R}}$, and it becomes quite visible in contrast to the narrow $\mathbf{R}$ matrix. A reduction of the width of the averaging kernels is not visible in Figures 3.16,3.18 and 3.20. It is quite remarkable though, that the extra-tropical stratospheric temperatures, seen in Figures 3.17 and 3.19, are allowed to depart considerably from the background in this run, bringing them closer to GRUAN temperatures.

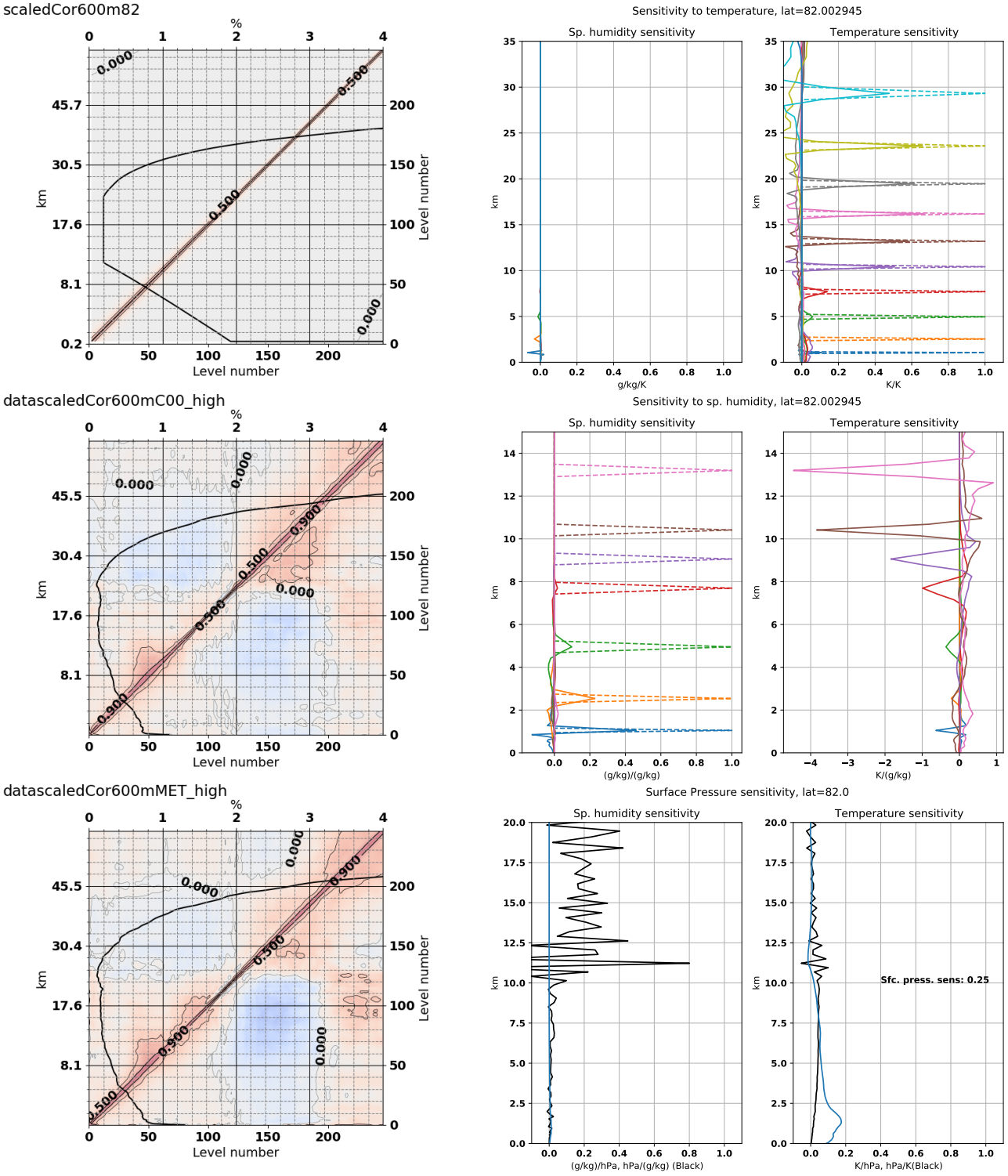


**Figure 3.16: Operational R-matrix with reduced correlation length, diagnostics at high latitudes**. **Left:** Error covariances, as in Fig. 3.1 for $|lat| > 60$ degrees. **Right:** Averaging kernels, as in Fig. 3.1, for $|lat| > 60$ degrees.

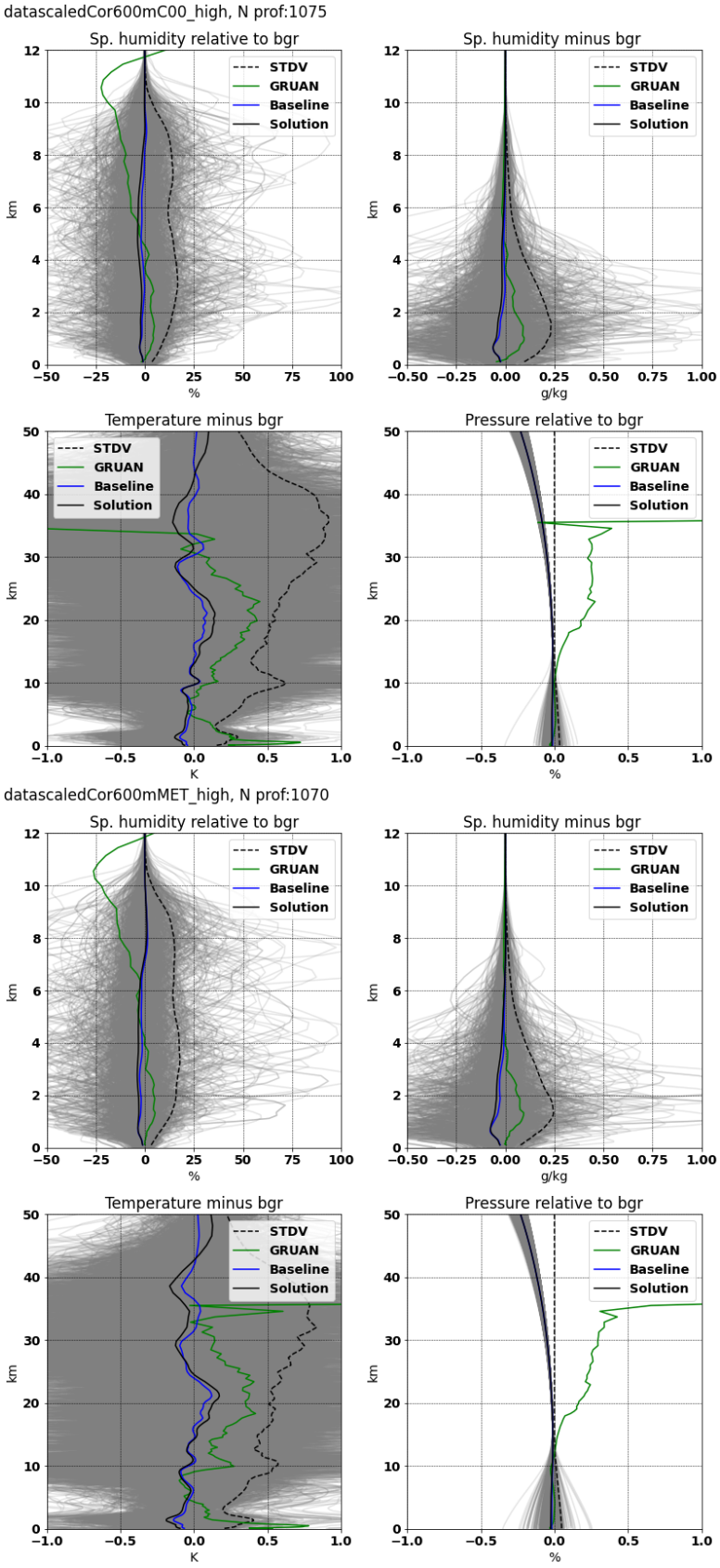


**Figure 3.17: Operational R-matrix with reduced correlation length, |lat|>60 degrees**. 1D-Var results (humidity, temperature and pressure, with background subtracted). Top: COSMIC. Bottom: Metop. Gray curves show solution, black: mean solution, blue: baseline, green: GRUAN and dashed: solution minus background STDV.

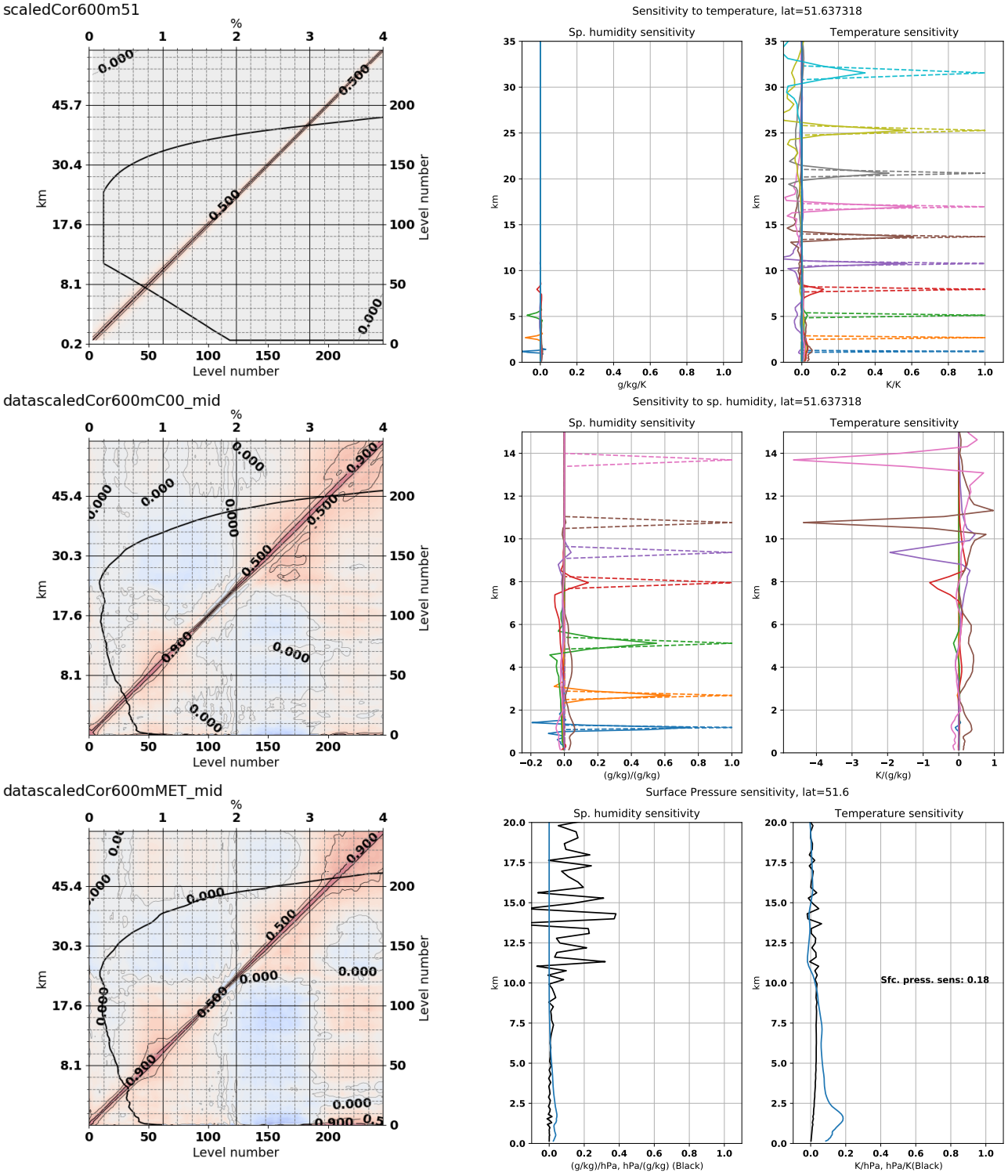


**Figure 3.18: Operational R-matrix with reduced correlation length, diagnostics at mid latitudes. Left:** Error covariances, as in Fig. 3.1 for $30 < |lat| < 60$ degrees. **Right:** Averaging kernels, as in Fig. 3.1, with $30 < |lat| < 60$ degrees.

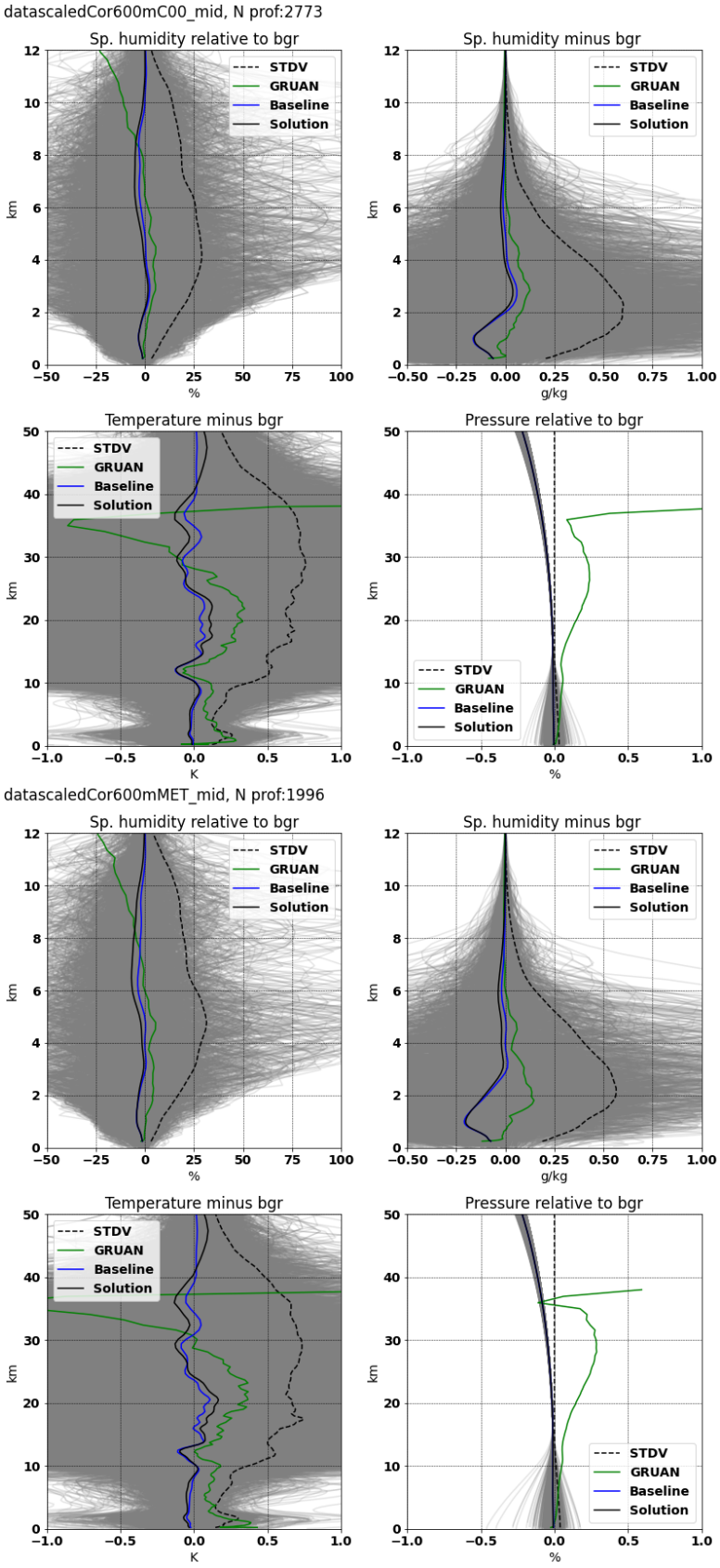


**Figure 3.19: Operational R-matrix with reduced correlation length, 30<|lat|<60 degrees**. 1D-Var results (humidity, temperature and pressure, with background subtracted) degrees. Top: COSMIC. Bottom: Metop. Gray curves show solution, black: mean solution, blue: baseline, green: GRUAN and dashed: solution minus background STDV.

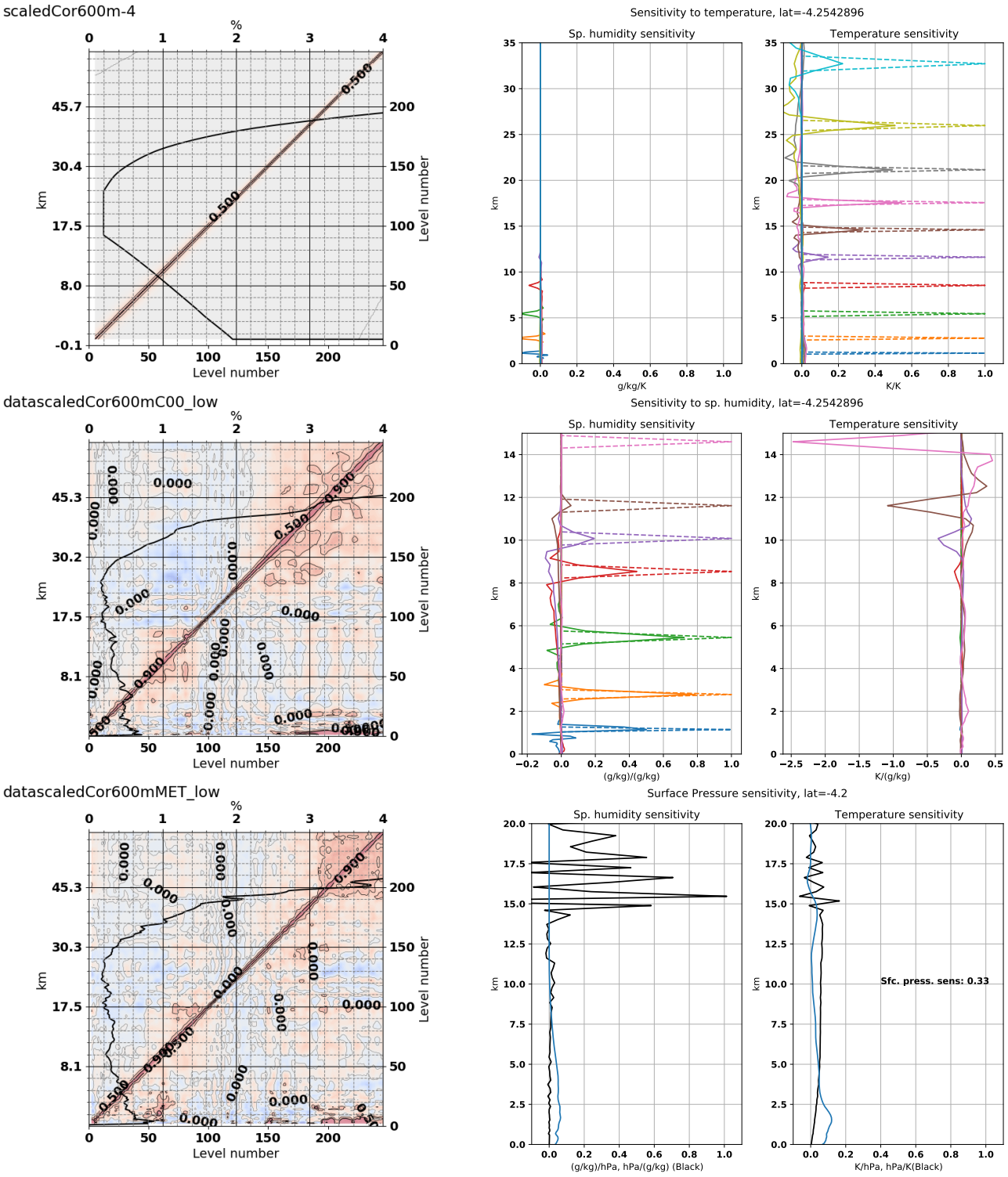


**Figure 3.20: Operational R-matrix with reduced correlation length, diagnostics at low latitudes**. **Left:** Error covariances, as in Fig. 3.1 for $|lat| < 30$ degrees. **Right:** Averaging kernels, as in Fig. 3.1, with $|lat| < 30$ degrees.

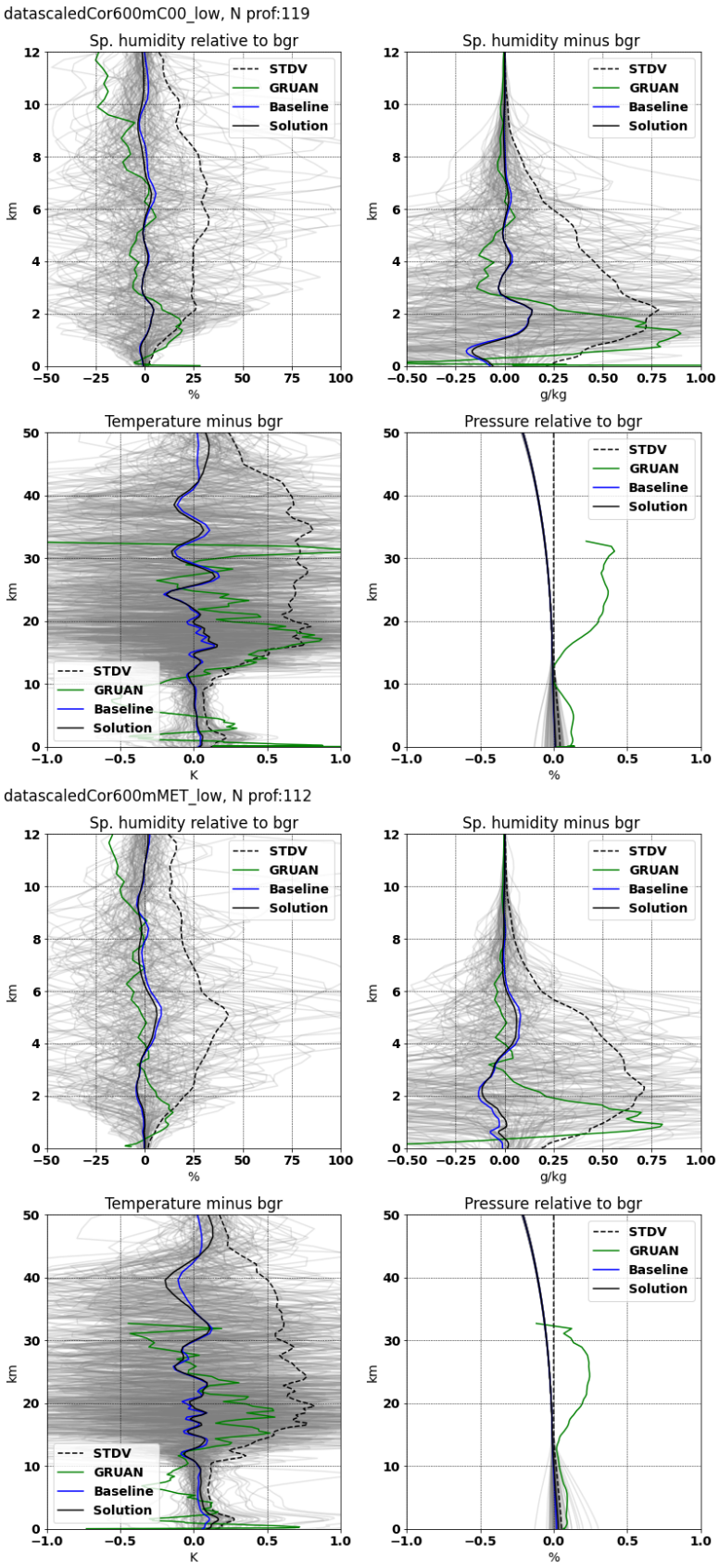


**Figure 3.21: Operational R-matrix with reduced correlation length, |lat|<30 degrees**. 1D-Var results (humidity, temperature and pressure, with background subtracted). Top: COSMIC. Bottom: Metop. Gray curves show solution, black: mean solution, blue: baseline, green: GRUAN and dashed: solution minus background STDV.

### 3.5 Troposphere focused R-matrix

The “troposphere focused” refractivity error covariance is designed with guidance from the three previous experiments. Again, the Desroziers matrices depends on what has been put into the 1D-Var, which also includes the background error covariance $\mathbf{B}$. So the Desroziers matrices from these experiments cannot be regarded as the truth, which can also be seen from the fact that they vary a lot. So what is being done here is just to note, on a qualitative level, the common tendencies in the Desroziers matrices, and then construct an $\mathbf{R}$ which combines the features of the previous Desroziers matrices, pointing to higher weighting of refractivity in the 1D-var:

1. Deflated standard deviation (0.1%)
2. Extension of the 0.1% regime down to 3 km.
3. Reduction of correlation length to 600 m

It is remarkable, that with this extremely low tropospheric standard deviation assumption, the Desroziers method suggests an even lower standard deviation. The Desroziers matrices arising from this experiment (Figures 3.22,3.24 and 3.26) show some very long range correlation patterns. In addition to the weak stratosphere-troposphere anticorrelation pattern, present in all experiments, a non-symmetric pattern (low right corner of especially Metop Desroziers matrices) is revealed as the refractivity standard deviation is allowed to drop even further, to 0.05%, at the surface.

The averaging kernels, Figures 3.22,3.24 and 3.26, naturally show high sensitivity in this experiment. The mid troposphere specific humidity sensitivity is almost 100%, but in the upper troposphere the temperature sensitivity dominates. The weighing between specific humidity and temperature is mainly determined by the B matrix.

Generally the baseline biases (Figures 3.23, 3.25 and 3.27) are enhanced as one would expect when combining the deflation of $\mathbf{R}$ with reduced correlation length, but at mid and high latitudes a remarkably strong dry bias of 10-15% is emerging, especially at mid latitudes between 6 and 10 km. The “tropospheric focus” experiment summarizes in which direction the radio occultation measurements points, if the background constraints are relaxed.

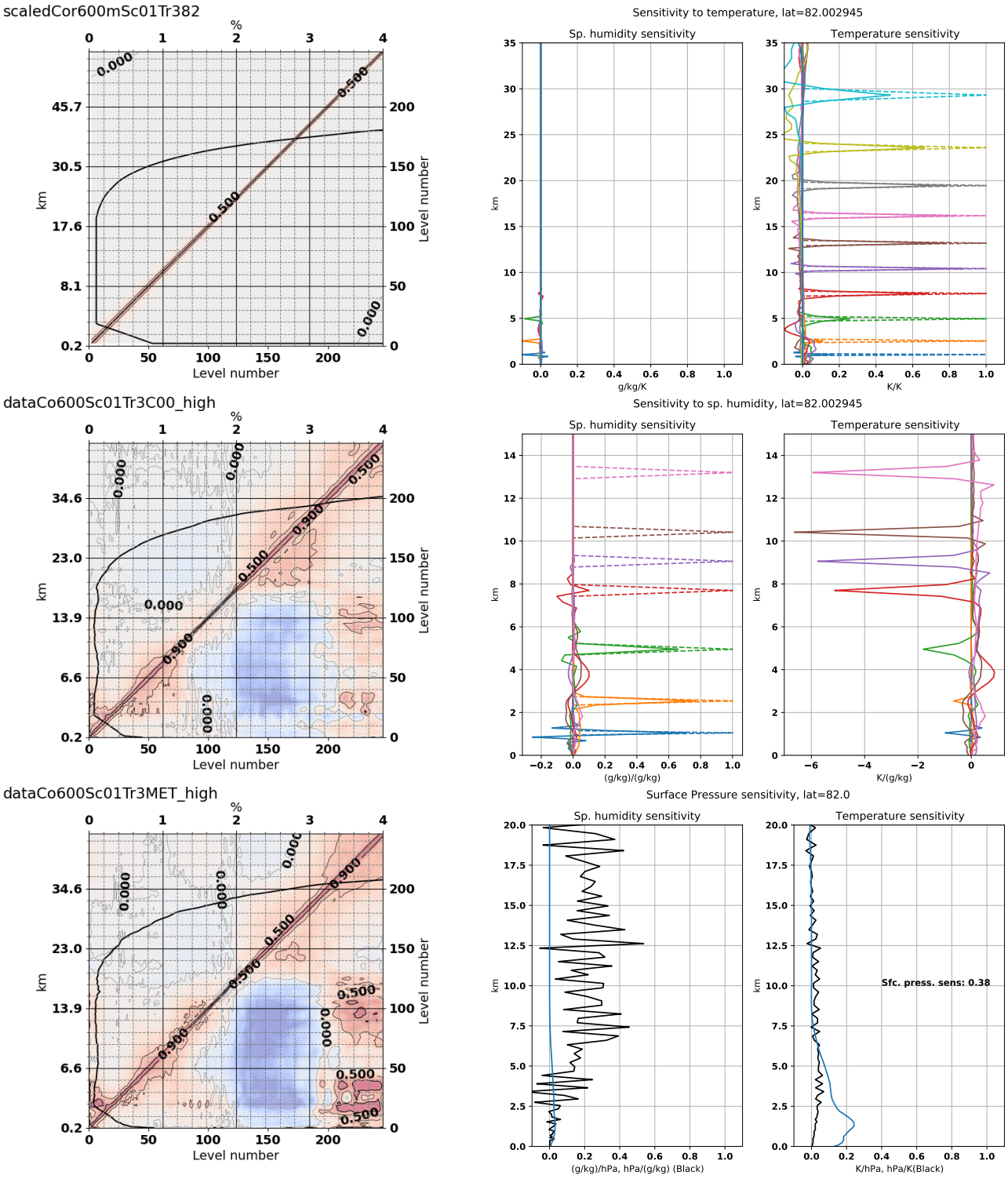


**Figure 3.22: Troposphere focused R-matrix, diagnostics at high latitudes**. **Left:** Error covariances, as in Fig. 3.1 for $|lat| > 60$ degrees. **Right:** Averaging kernels, as in Fig. 3.1, for $|lat| > 60$ degrees.

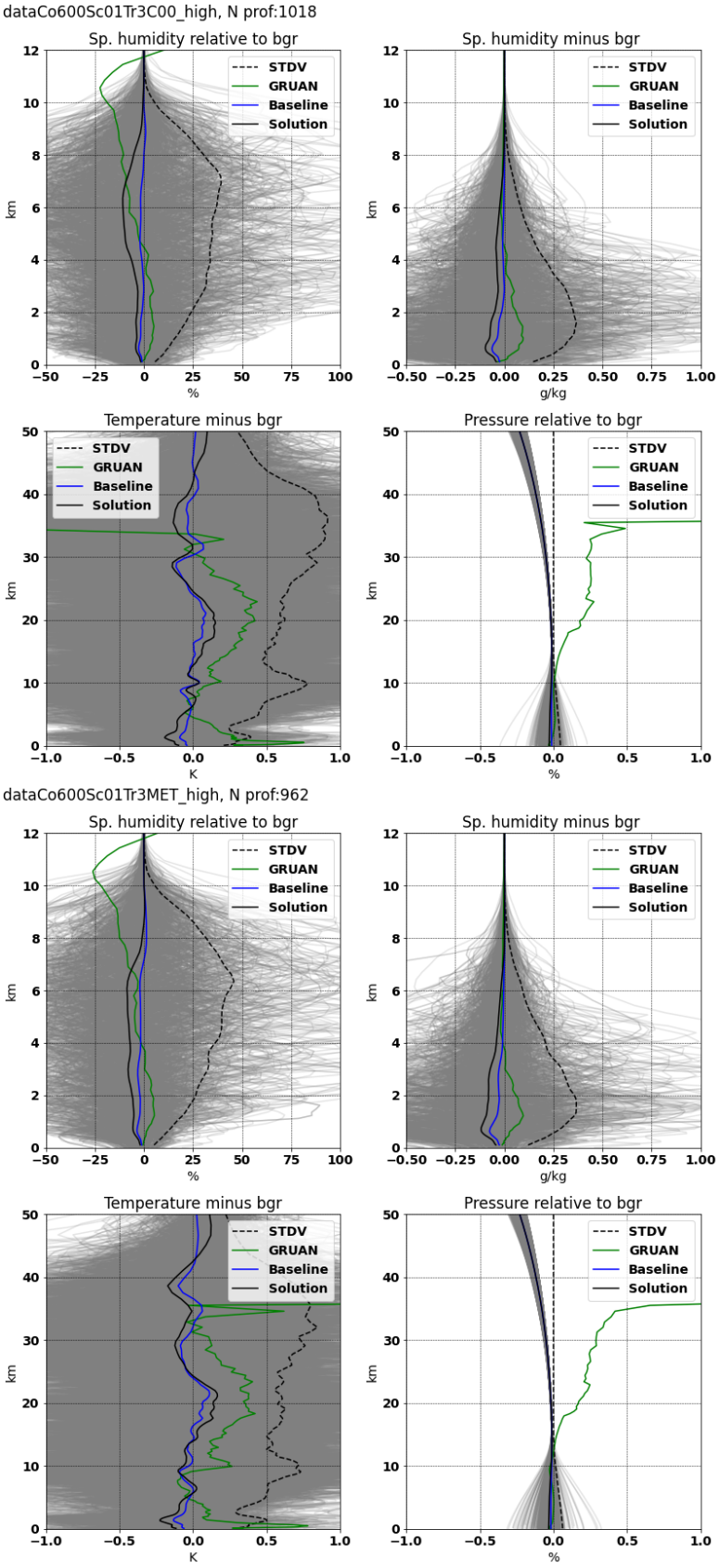


**Figure 3.23: Troposphere focused R-matrix, |lat|>60 degrees**. 1D-Var results (humidity, temperature and pressure, with background subtracted). Top: COSMIC. Bottom: Metop. Gray curves show solution, black: mean solution, blue: baseline, green: GRUAN and dashed: solution minus background STDV.

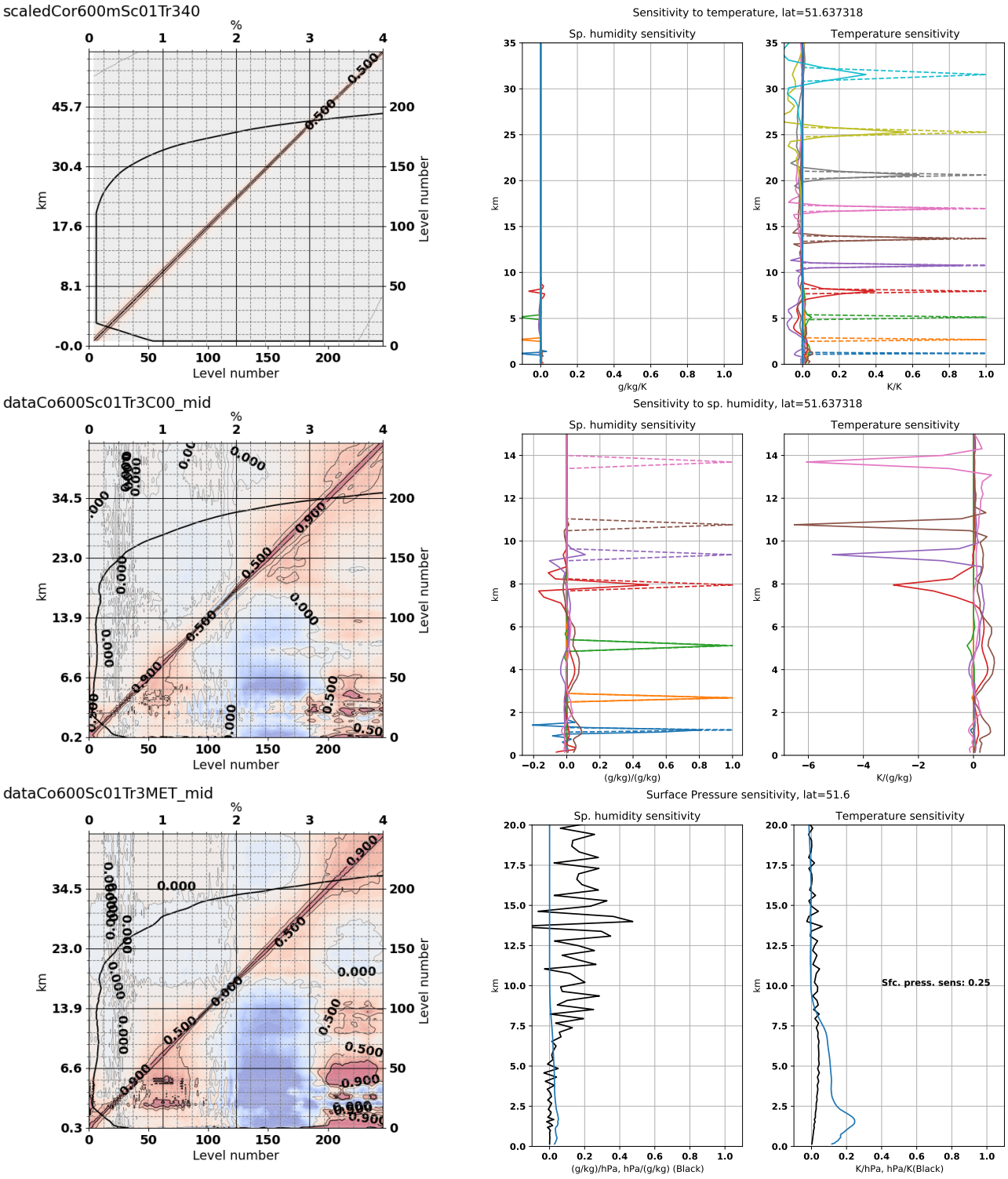


**Figure 3.24: Troposphere focused R-matrix, diagnostics at mid latitudes**. **Left:** Error covariances, as in Fig. 3.1 for $30 < |lat| < 60$ degrees. **Right:** Averaging kernels, as in Fig. 3.1, with $30 < |lat| < 60$ degrees.

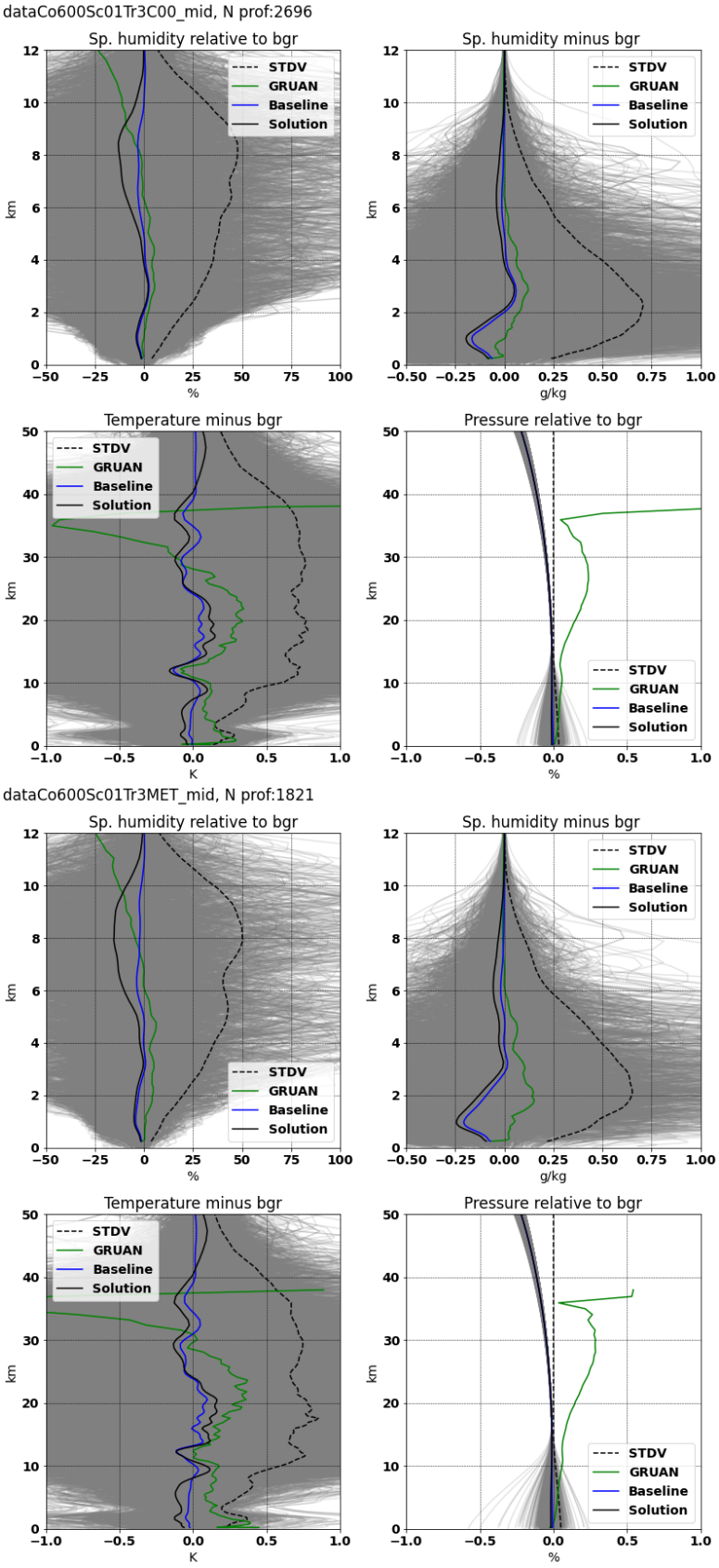


**Figure 3.25: Troposphere focused R-matrix, 30<|lat|<60 degrees**. 1D-Var results (humidity, temperature and pressure, with background subtracted) degrees. Top: COSMIC. Bottom: Metop. Gray curves show solution, black: mean solution, blue: baseline, green: GRUAN and dashed: solution minus background STDV.

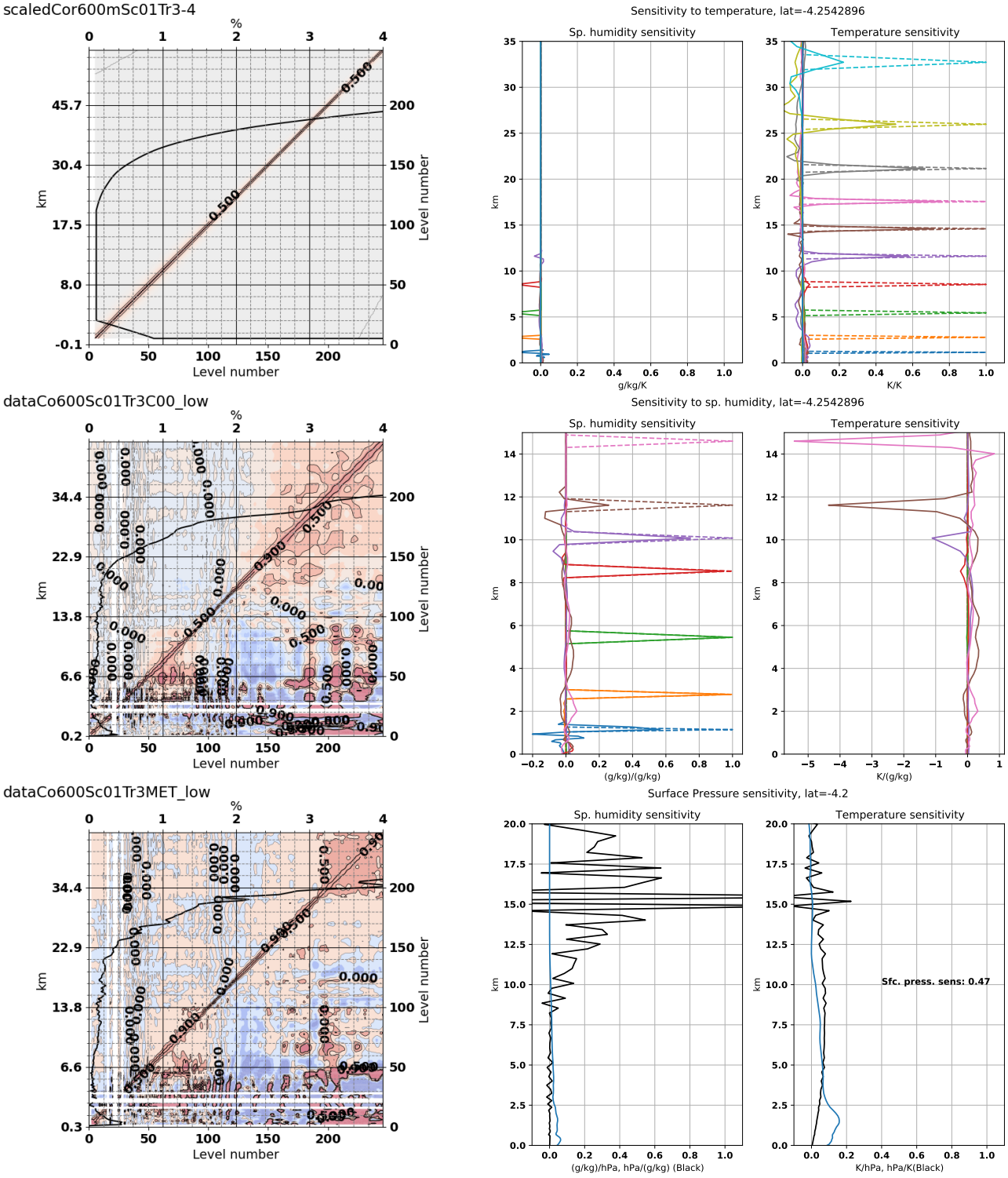


**Figure 3.26: Troposphere focused R-matrix, diagnostics at low latitudes**. **Left:** Error covariances, as in Fig. 3.1 for $|lat| < 30$ degrees. **Right:** Averaging kernels, as in Fig. 3.1, with $|lat| < 30$ degrees.

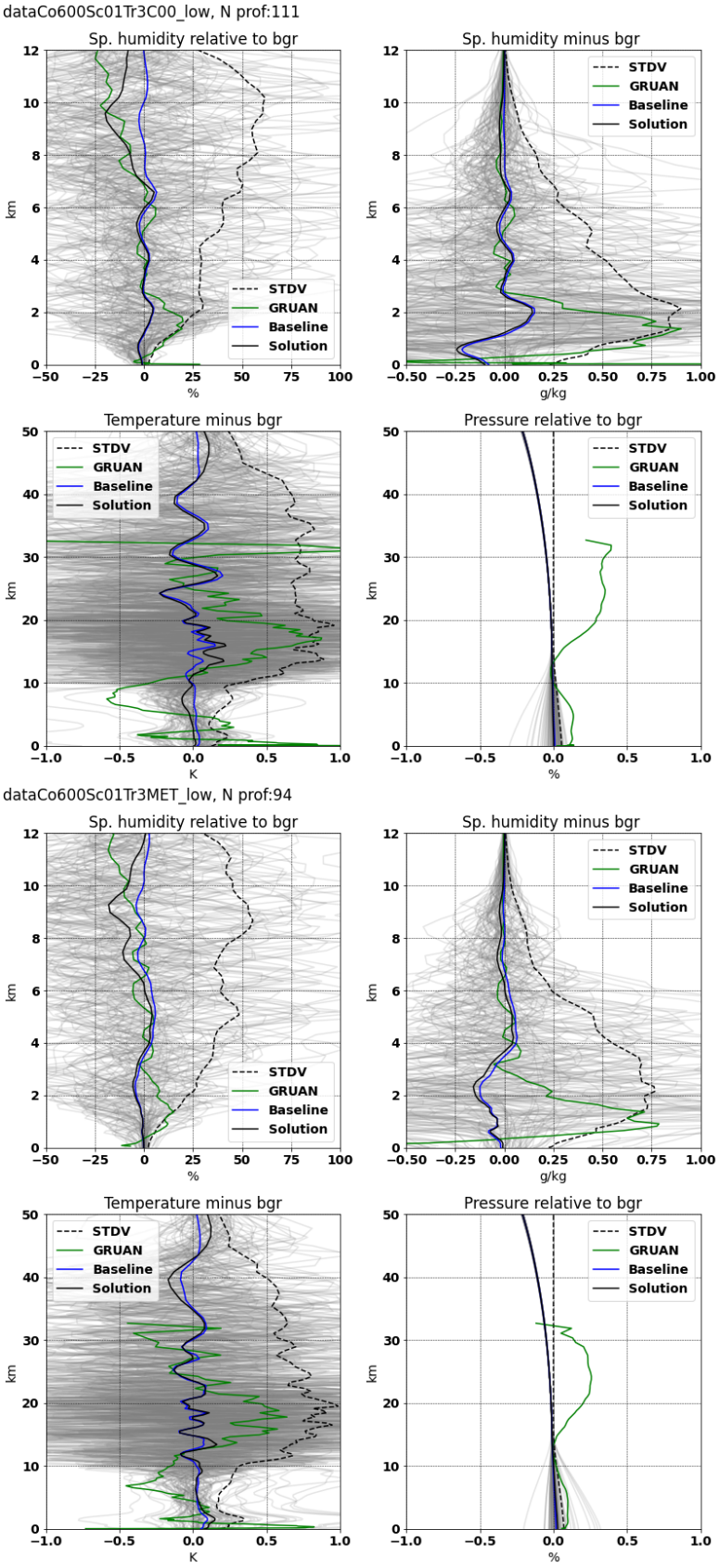


**Figure 3.27: Troposphere focused R-matrix, |lat|<30 degrees**. 1D-Var results (humidity, temperature and pressure, with background subtracted). Top: COSMIC. Bottom: Metop. Gray curves show solution, black: mean solution, blue: baseline, green: GRUAN and dashed: solution minus background STDV.

## 3.6 ECMWF operational

Finally this and the following section show results based on refractivity error covariance matrices provided by ECMWF. At ECMWF the 4D-Var assimilation scheme ingests bending angle data from Metop A, B and C, using a diagonal bending angle error covariance matrix, which is designed to be a little “conservative” (meaning high diagonal values) to support robustness of the ECMWF assimilation system. The bending angle standard deviation is constructed in the same way as the refractivity standard deviation in the ROM SAF. That is, a constant relative error (here 1.25%) is assumed above the tropopause (in this case fixed at 10 km). Below the tropopause the error increases linearly to 20% at 0 km impact height. The error is not allowed to drop below 3 $\mu$rad. The refractivity matrix tested here has been constructed by mapping bending angle error covariance $\mathbf{R}_{BA}$ to refractivity error covariance through $\mathbf{R} = \mathbf{A}\mathbf{R}_{BA}\mathbf{A}^T$, where $\mathbf{A}$ is a linarized descrete Abel transform.

The refractivity covariance matrix (left plot of Figure 3.28) is only slightly more conservative than the operational ROM SAF refractivity covariance matrix in the lower stratosphere, and above approximately 25 km the ECMWF standard deviation is in fact lower then the ROM SAF covariance (compare eg. Figures 3.30 and 3.2. The correlation length of the ECMWF $\mathbf{R}$ matrix is generally lower (i.e. less conservative) than the 3 km ROM SAF correlation length. The derived Desroziers matrices in Figures 3.28,3.30 and 3.32 suggest that the ECMWF correlation length, calculated from a diagonal bending angle covariance, is an underestimate of the refractivity correlation length. Especially in the stratosphere around 30-40 km and near the tropopasue.

The troposphere performance is also interesting. Due to a less correlated $\mathbf{R}$, the ECMWF allows more impact in upper troposphere at midlatitudes than the ROM SAF does, which is seen in the specific humidity in Fig. 3.31. It was shown in the reduced correlation length experiment that lower correlation length in $\mathbf{R}$ leads to increased specific humidity (negative) bias, and it seems plausible that this is what is going on here also. This increase in sensitivity is not really seen in the averaging kernels, but is quite clear in the bias plots.

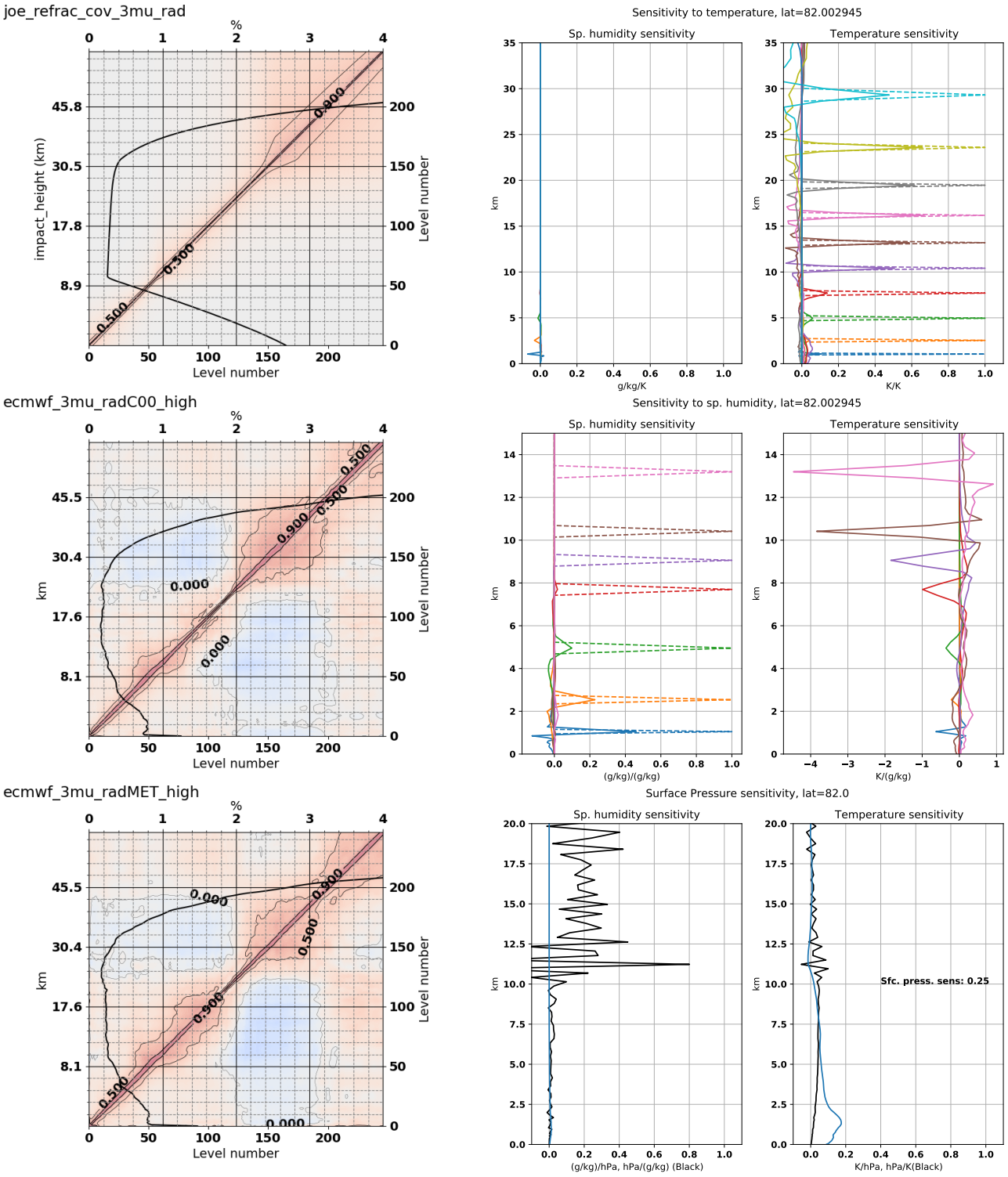


**Figure 3.28: ECMWF operational, diagnostics at high latitudes**. **Left:** Error covariances, as in Fig. 3.1 for $|lat| > 60$ degrees. **Right:** Averaging kernels, as in Fig. 3.1, for $|lat| > 60$ degrees.

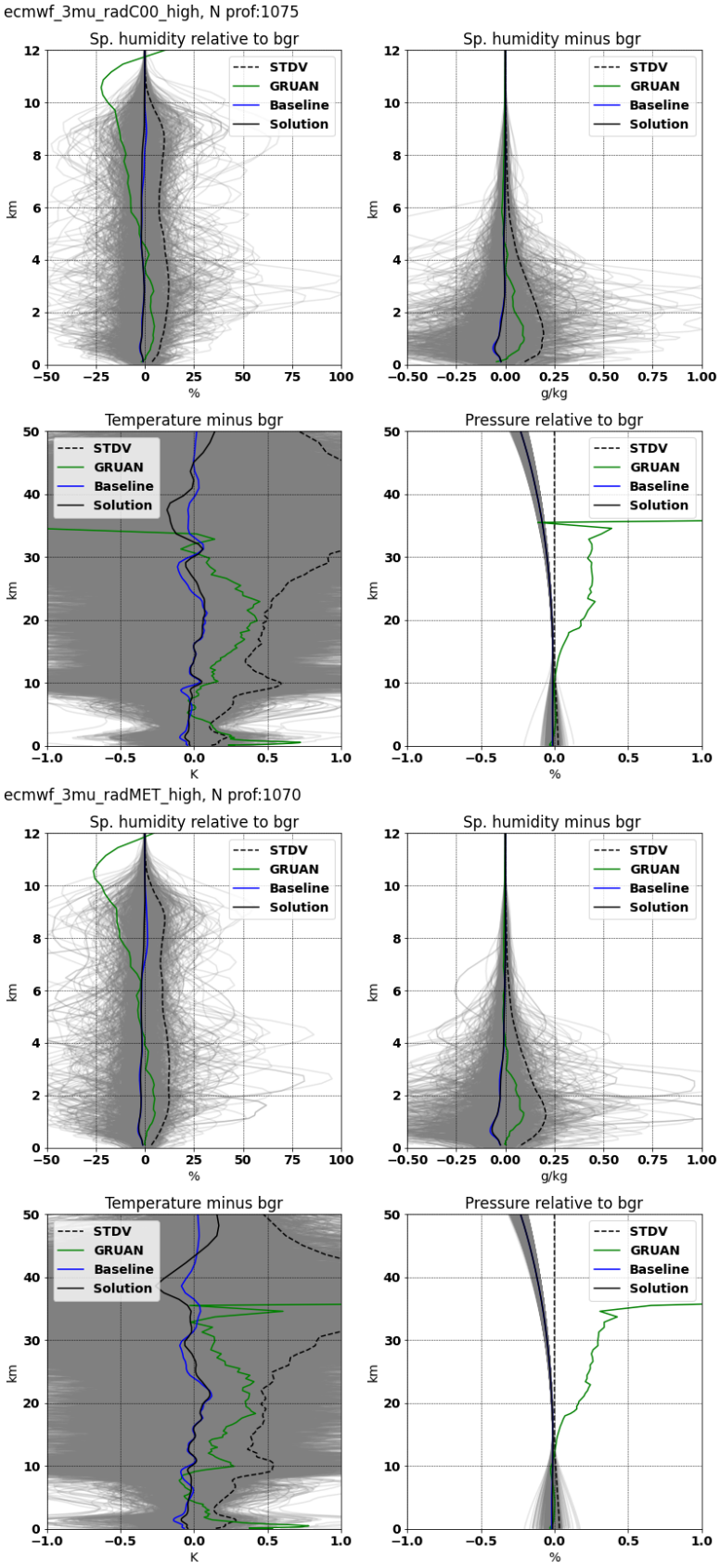


**Figure 3.29: ECMWF operational, |lat|>60 degrees**. 1D-Var results (humidity, temperature and pressure, with background subtracted). Top: COSMIC. Bottom: Metop. Gray curves show solution, black: mean solution, blue: baseline, green: GRUAN and dashed: solution minus background STDV.

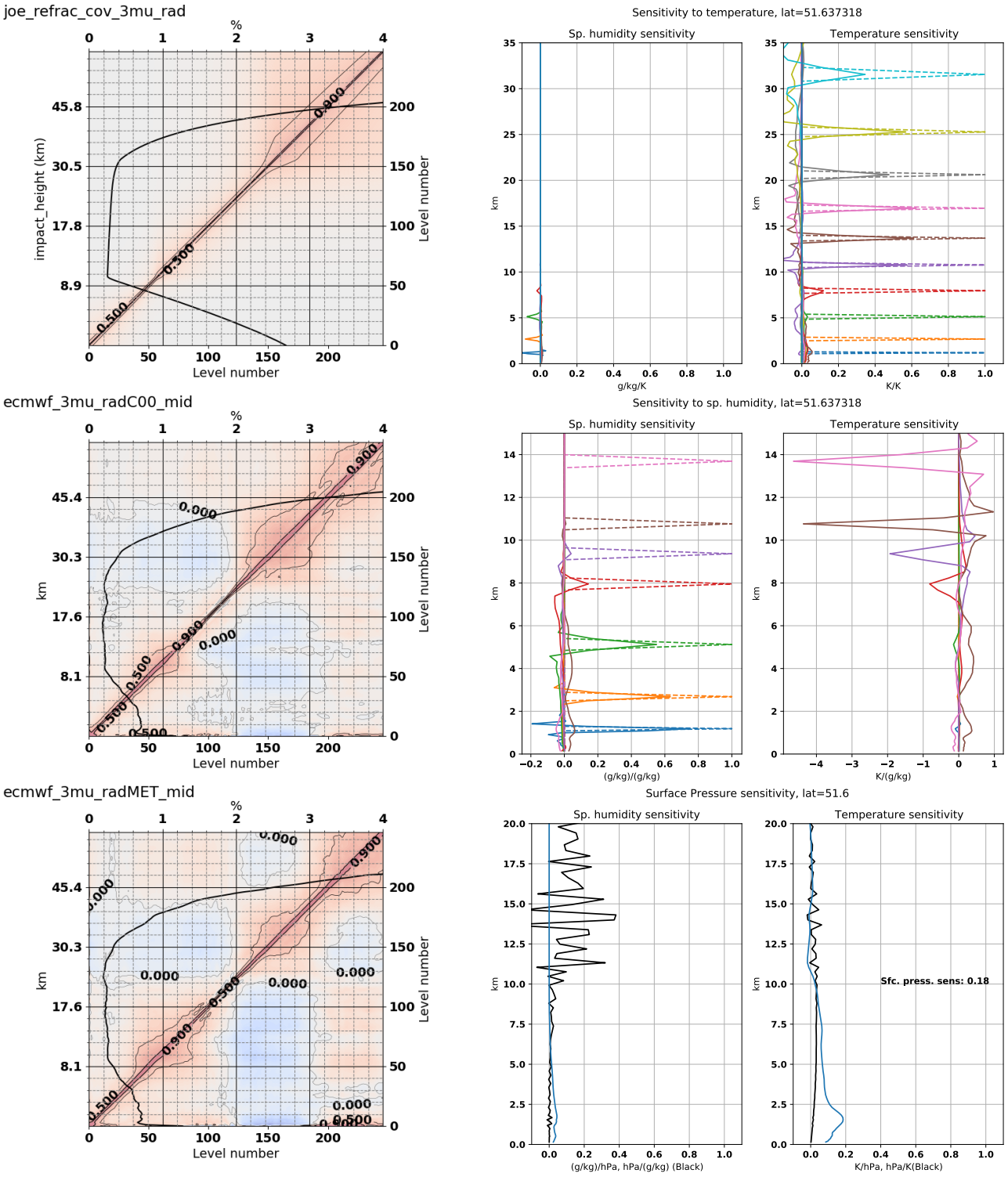


**Figure 3.30: ECMWF operational, diagnostics at mid latitudes**. **Left:** Error covariances, as in Fig. 3.1 for $30 < |lat| < 60$ degrees. **Right:** Averaging kernels, as in Fig. 3.1, with $30 < |lat| < 60$ degrees.

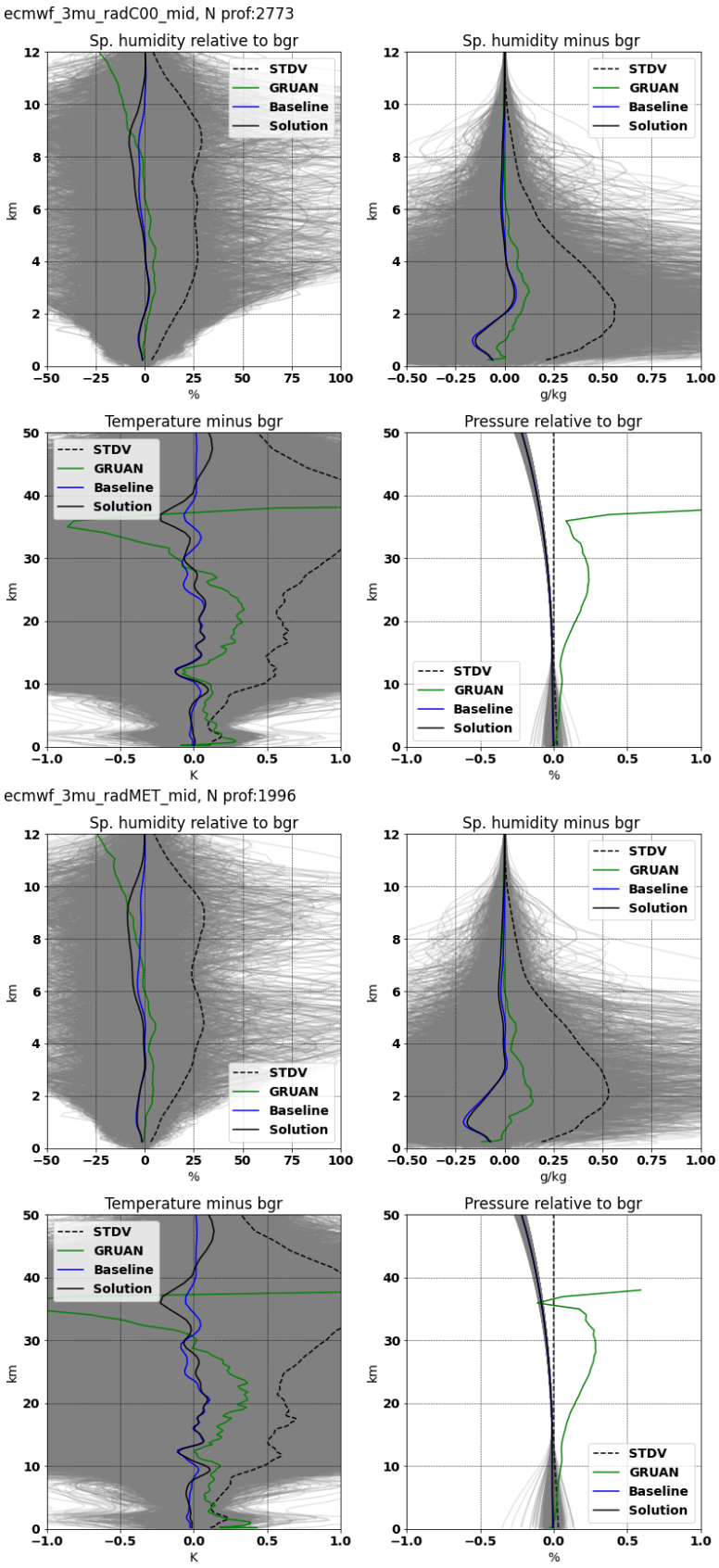


**Figure 3.31: ECMWF operational, 30<|lat|<60 degrees**. 1D-Var results (humidity, temperature and pressure, with background subtracted) degrees. Top: COSMIC. Bottom: Metop. Gray curves show solution, black: mean solution, blue: baseline, green: GRUAN and dashed: solution minus background STDV.

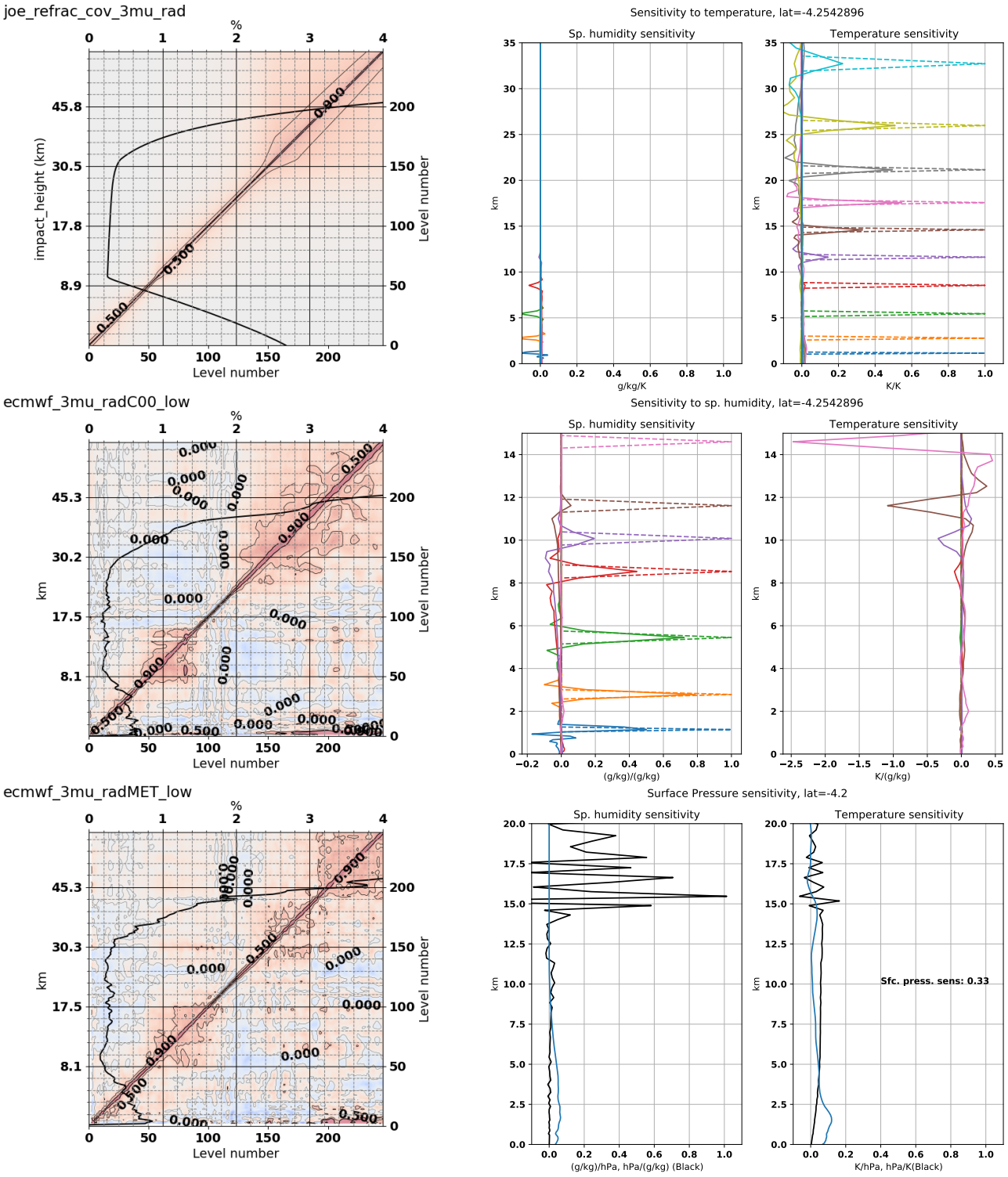


**Figure 3.32: ECMWF operational, diagnostics at low latitudes**. **Left:** Error covariances, as in Fig. 3.1 for $|lat| < 30$ degrees. **Right:** Averaging kernels, as in Fig. 3.1, with $|lat| < 30$ degrees.

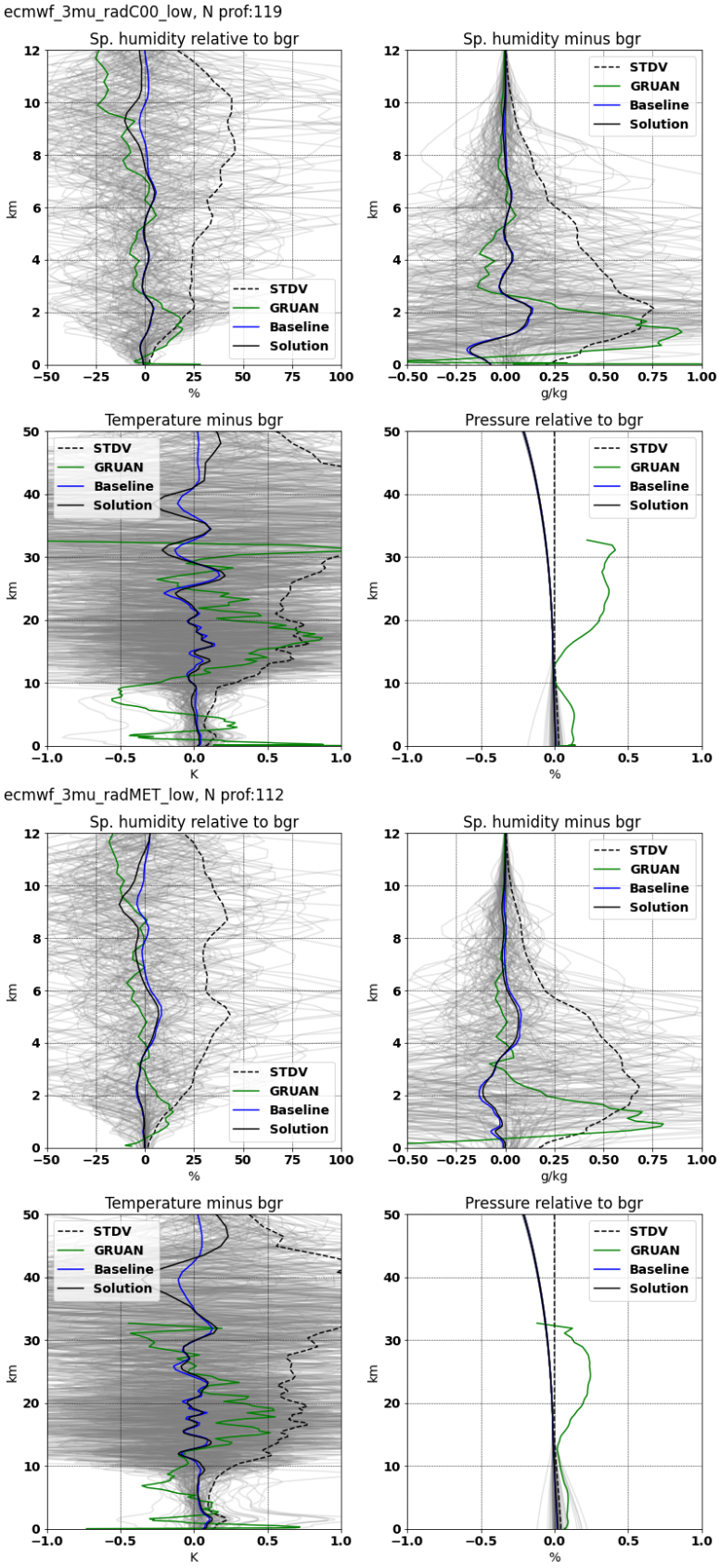


**Figure 3.33: ECMWF operational, |lat|<30 degrees**. 1D-Var results (humidity, temperature and pressure, with background subtracted). Top: COSMIC. Bottom: Metop. Gray curves show solution, black: mean solution, blue: baseline, green: GRUAN and dashed: solution minus background STDV.

### 3.7 ECMWF, min 1 $\mu$rad

This run is completely identical to the previous, except that the minimum bending angle error is set to 1 $\mu$rad. This has only impact on high altitudes. The Desroziers correlations are a bit increased at high altitude in Figures 3.28,3.30 and 3.32). In all the Figures 3.35,3.37 and 3.39) 1D-Var temperatures are strongly cold biased around 40 km (-0.7 K compared to ERA5 at high and mid-latitudes), and at the same time the Desroziers matrices are strongly correlated at that altitude. The ECMWF min 1 $\mu$rad error covariance allows RO to have a relatively strong impact at high altitude.

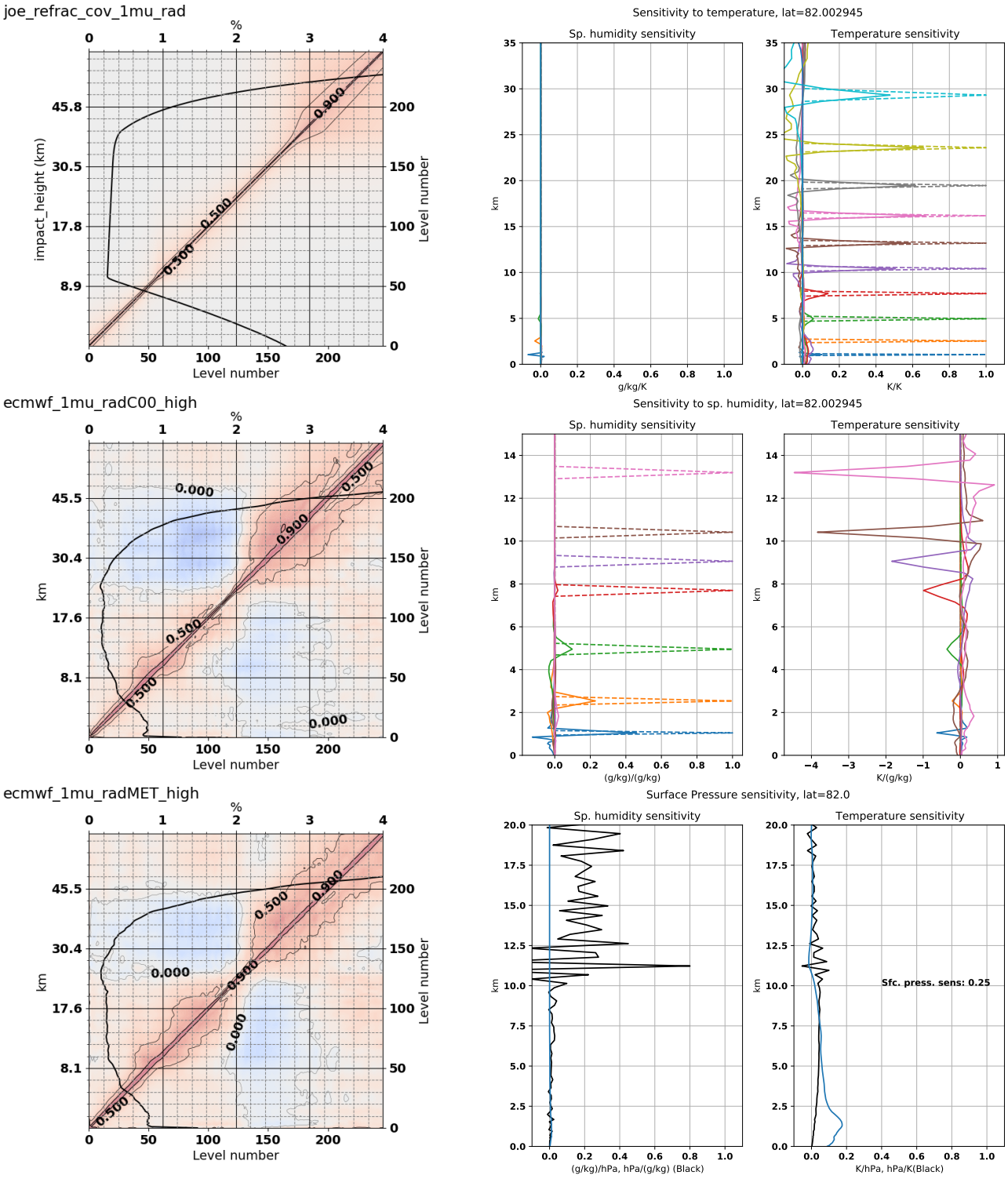


**Figure 3.34: ECMWF, min 1 $\mu$rad, diagnostics at high latitudes**. **Left:** Error covariances, as in Fig. 3.1 for $|lat| > 60$ degrees. **Right:** Averaging kernels, as in Fig. 3.1, for $|lat| > 60$ degrees.

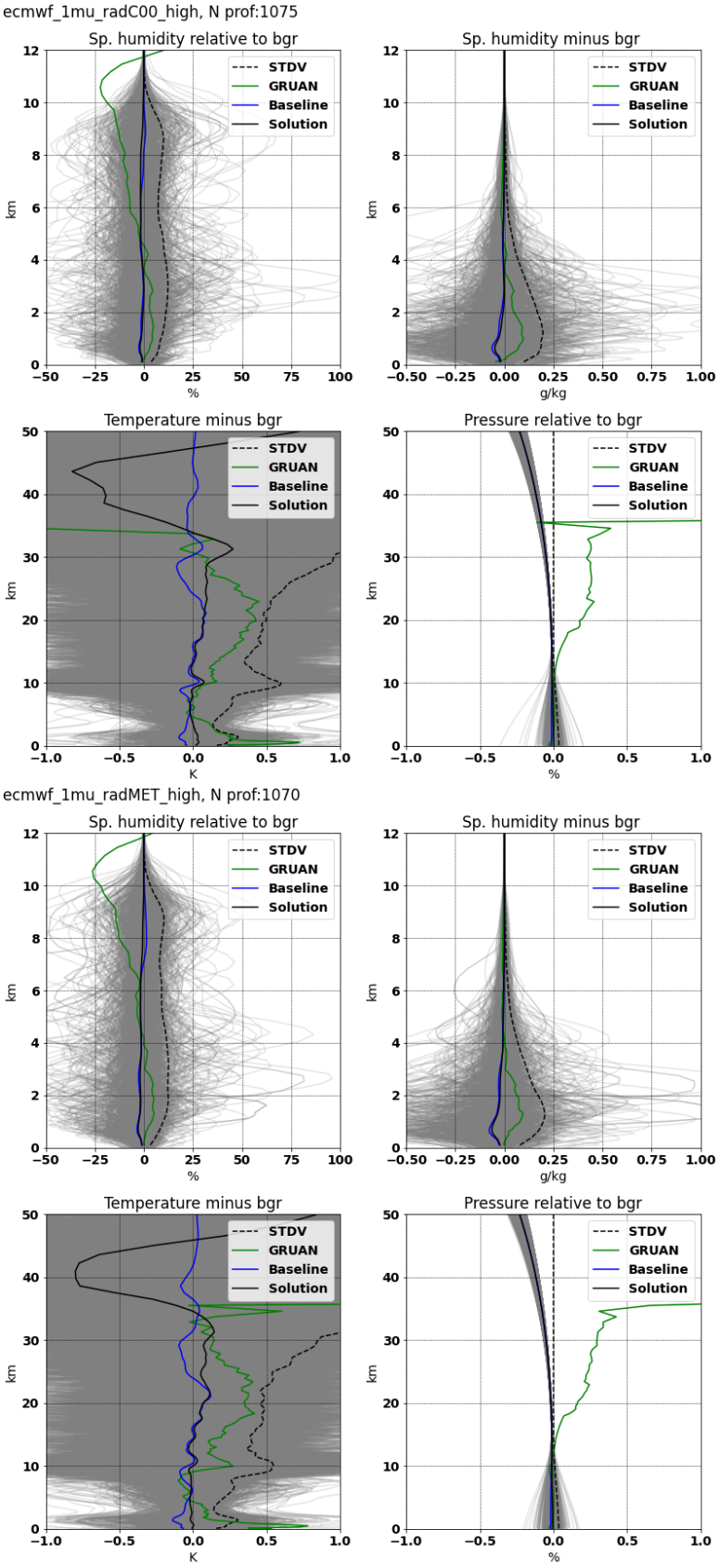


**Figure 3.35: ECMWF, min 1 $\mu$rad, |lat|>60 degrees**. 1D-Var results (humidity, temperature and pressure, with background subtracted). Top: COSMIC. Bottom: Metop. Gray curves show solution, black: mean solution, blue: baseline, green: GRUAN and dashed: solution minus background STDV.

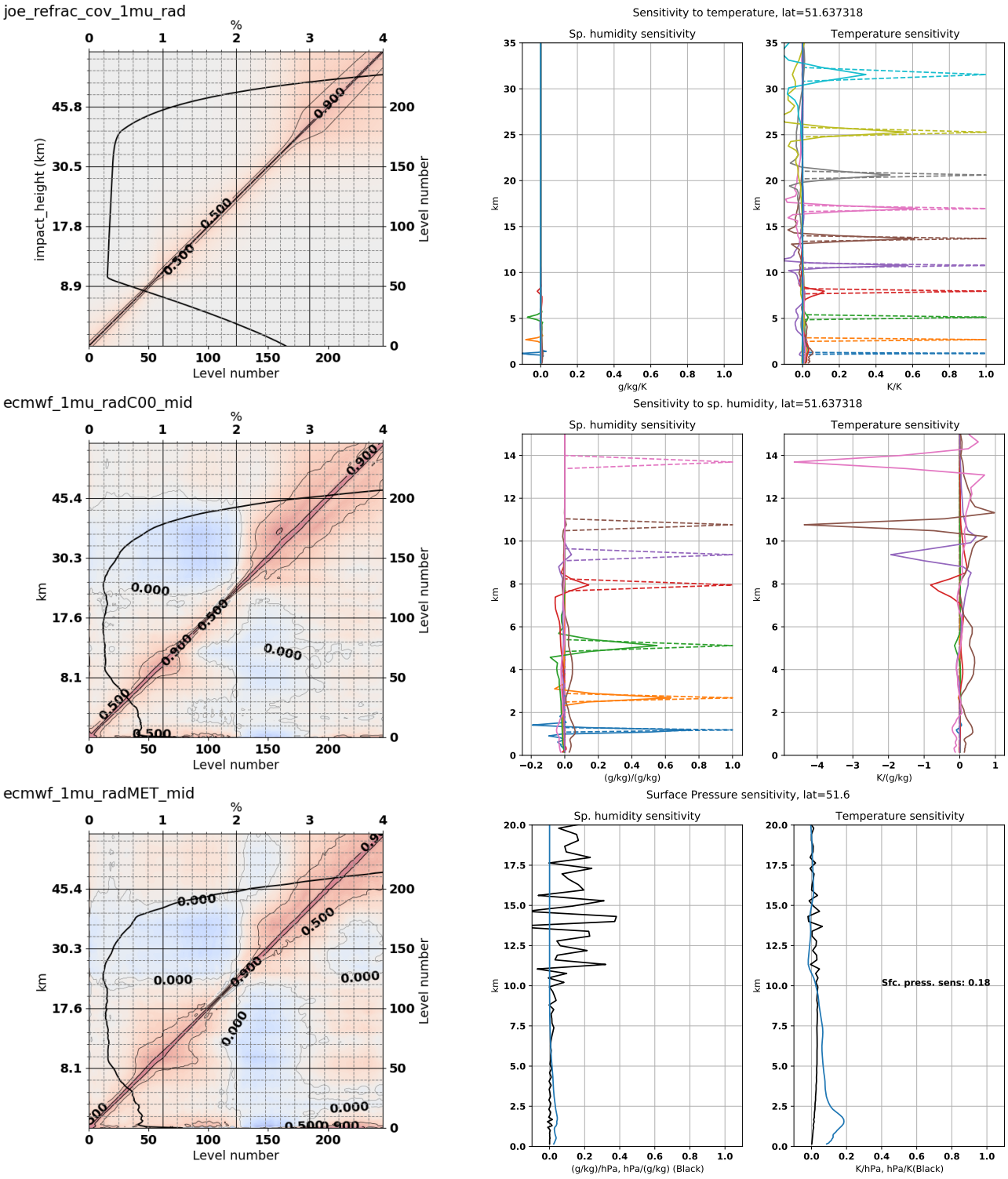


**Figure 3.36: ECMWF, min 1 $\mu$rad, diagnostics at mid latitudes**. **Left:** Error covariances, as in Fig. 3.1 for $30 < |lat| < 60$ degrees. **Right:** Averaging kernels, as in Fig. 3.1, with $30 < |lat| < 60$ degrees.

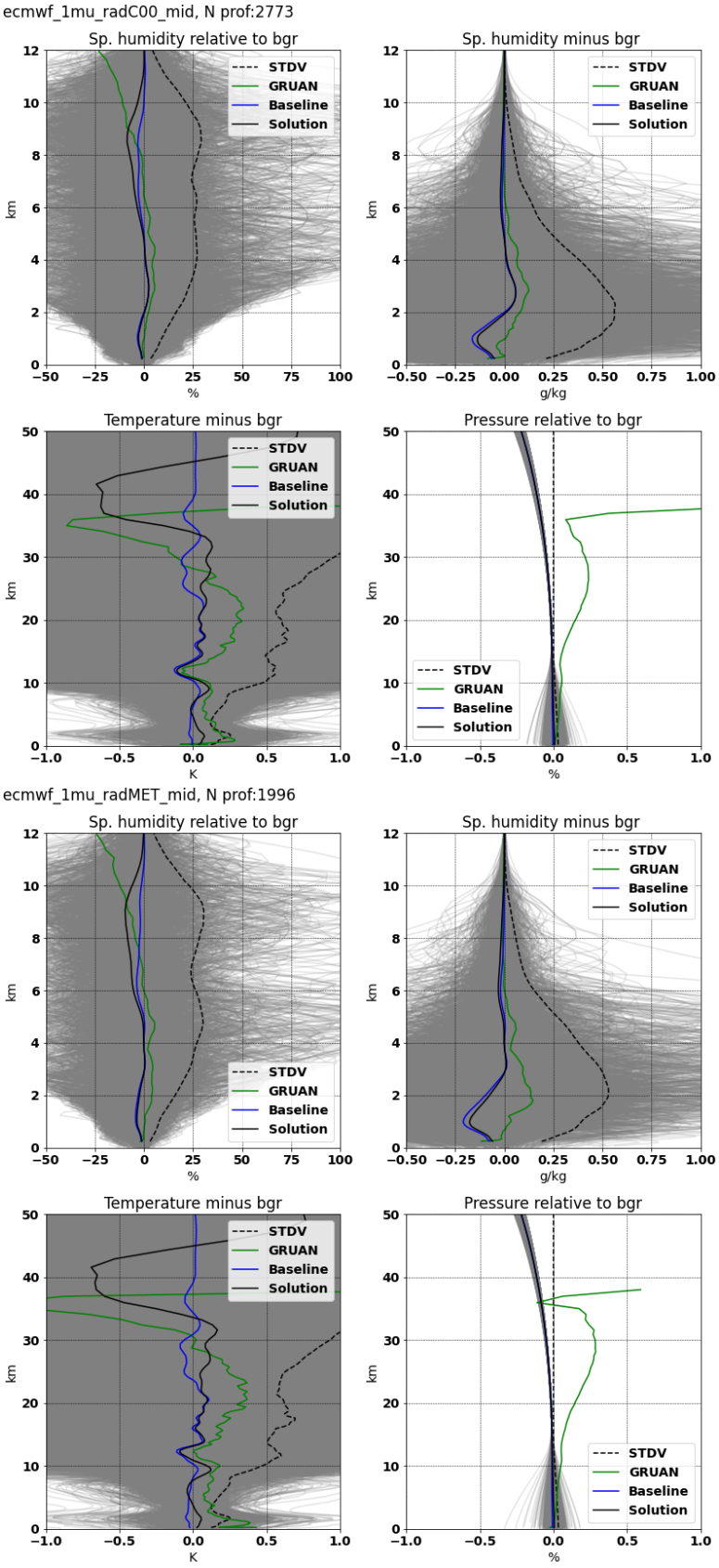


**Figure 3.37: ECMWF, min 1 $\mu$rad, 30<|lat|<60 degrees**. 1D-Var results (humidity, temperature and pressure, with background subtracted) degrees. Top: COSMIC. Bottom: Metop. Gray curves show solution, black: mean solution, blue: baseline, green: GRUAN and dashed: solution minus background STDV.

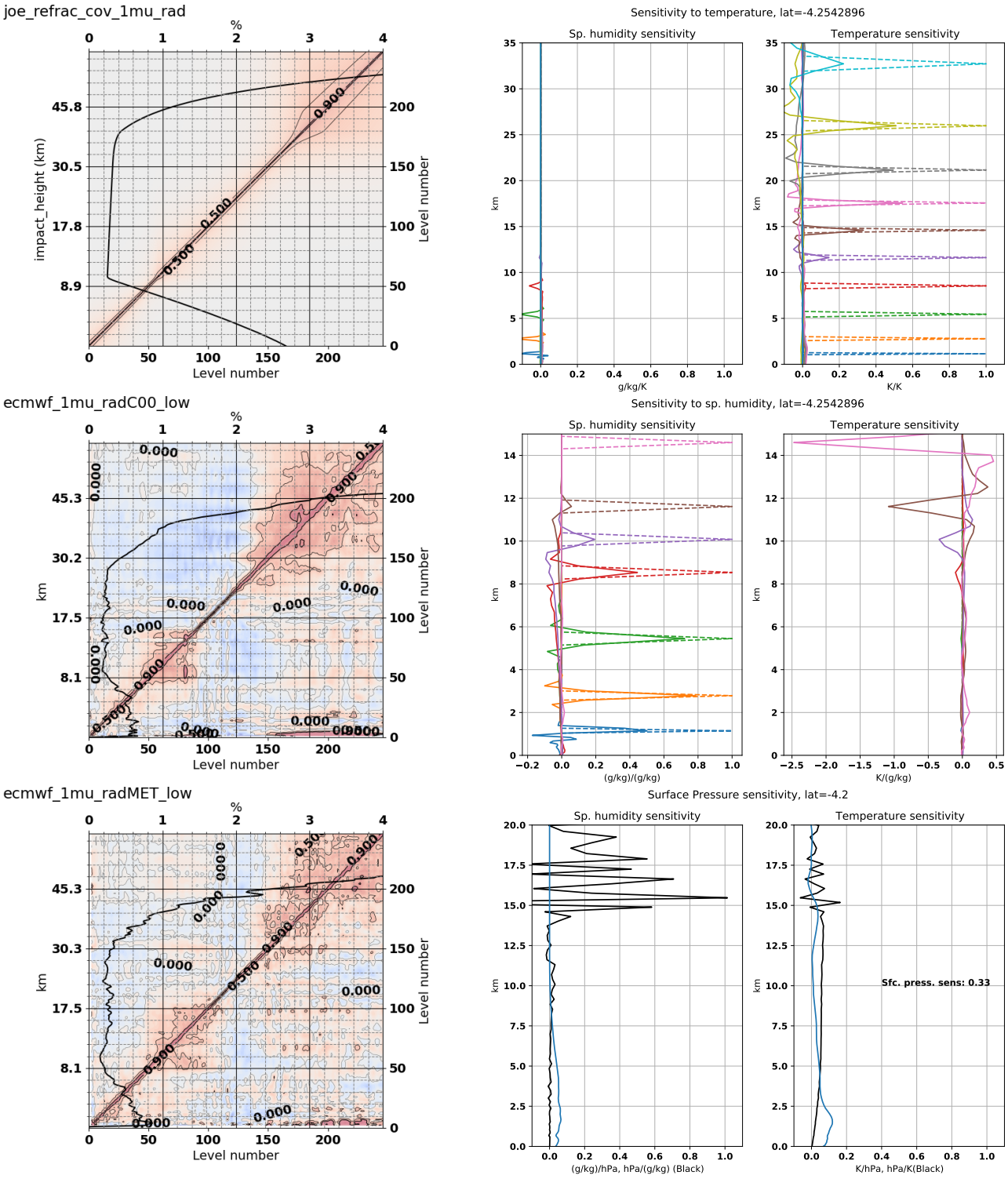


**Figure 3.38: ECMWF, min 1 $\mu$rad, diagnostics at low latitudes**. **Left:** Error covariances, as in Fig. 3.1 for $|lat| < 30$ degrees. **Right:** Averaging kernels, as in Fig. 3.1, with $|lat| < 30$ degrees.

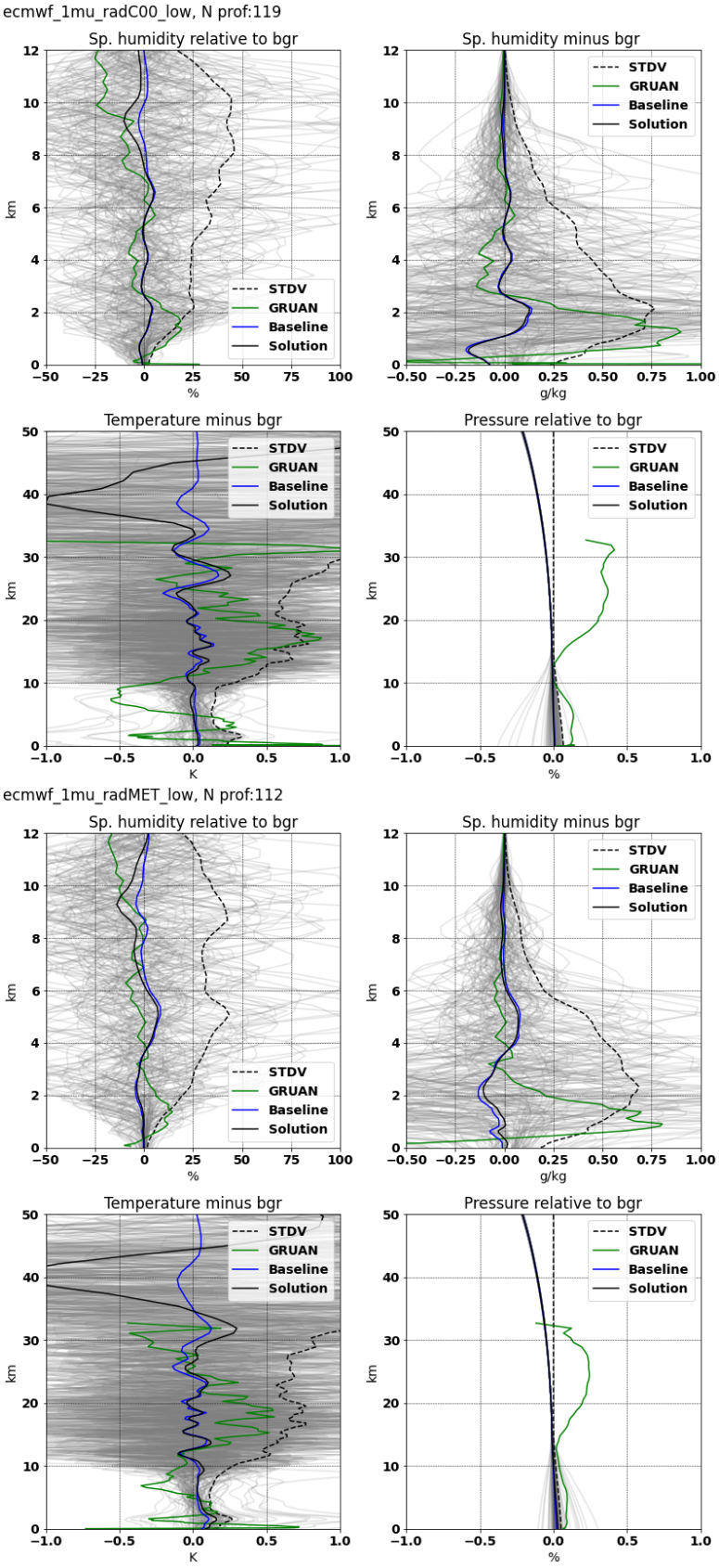


**Figure 3.39: ECMWF, min 1 $\mu$rad, |lat|<30 degrees**. 1D-Var results (humidity, temperature and pressure, with background subtracted). Top: COSMIC. Bottom: Metop. Gray curves show solution, black: mean solution, blue: baseline, green: GRUAN and dashed: solution minus background STDV.

# 4 Sensitivity of Desroziers matrix estimates to assumed R-matrix

In this chapter a summary of the estimated Desroziers diagonals (variances) is presented and conclusions are drawn from the dependency of the Desroziers estimate $\tilde{\mathbf{R}}$, on the input refractivity error variance $\mathbf{R}$.

Looking first at Figure 4.1, showing $\tilde{\mathbf{R}}$ diagonals as function of height, the following features are noted: The $\tilde{\mathbf{R}}$ diagonals differ from each other, which is to be expected when using different $\mathbf{R}$ as input. Especially at low altitudes, below 25 km, there is a substantial split up of the estimated variances. Above 30 km there is different split, where the variance of COSMIC-1 is seen to be larger than the variance of Metop, especially at Mid and High latitudes. This will not be discussed further here, but it is noted that the COSMIC-Metop difference is consistent with what was observed in the validation of the ROM SAF CDR-v1.0 data ([10] page 25).

Diagonal elements of $\tilde{\mathbf{R}}$, $\sigma^2_{\mathbf{des}}$ are plotted as function of input variances $\sigma^2_{\mathbf{inp}}$ for a few selected altitudes in Figure 4.2. Metop (blue) and COSMIC-1 (red) results can be viewed separately. It is noted that $\sigma^2_{\mathbf{des}}$ is generally lower than the assumed covariance diagonals, $\sigma^2_{\mathbf{inp}}$. At high altitudes (around 30 and 40 km), at mid and high latitudes, there is almost no dependence on $\sigma^2_{\mathbf{inp}}$. At low altitudes, and in the tropics there is generally a positive dependency such that $\sigma^2_{\mathbf{des}}$ increases with $\sigma^2_{\mathbf{inp}}$, but levels off at a low fraction of $\sigma^2_{\mathbf{inp}}$.

All the experiments presented in Chapter 3 are performed with the same set of background error uncertainty $\mathbf{B}$, and varying observation uncertainty $\mathbf{R}$. The question is now what can be inferred about the true $\mathbf{B}$ and $\mathbf{R}$ from these results:

In [1] the observation error covariance is written on the form

$$\tilde{\mathbf{R}} = \mathbf{R}(\mathbf{HBH^T} + \mathbf{R})^{-1}(\mathbf{HB^*H^T} + \mathbf{R^*}), \tag{4.1}$$

where $\mathbf{B}^*$ and $\mathbf{R}^*$ are the true error covariances, and $\mathbf{B}$ and $\mathbf{R}$ are the assumed error covariances. The term $\mathbf{HB^*H^T} + \mathbf{R^*}$ may be estimated empirically. Equation 4.1 is valid for the diagonals separately, since its derivation can be carried out for a one dimensional single layer case.

In Figure 4.3 a diagonal term of equation 4.1 is plotted in a normalized way, corresponding to setting the sum of the true variances $\sigma_b^{2^*} + \sigma^{2^*}$ equal to unity. The plot shows the relation between an estimated diagonal element $\widetilde{\sigma^2}$ from the $\tilde{\mathbf{R}}$ matrix and an assumed diagonal element $\sigma^2$ from the $\mathbf{R}$ matrix [1]. This approach is consistent what is being used in [5], where $\tilde{\mathbf{R}}$ is expressed in terms of the difference beteeen the true and the assumed $\mathbf{B}$.

It is seen that $\widetilde{\sigma^2}$ is always an increasing function of $\sigma^2$, leveling off at $\sigma_b^{2^*} + \sigma^{2^*}$. If $\widetilde{\sigma^2}$ is lower than $\sigma^2$ for all choices of $\sigma^2$, it is a signature of $\sigma_b^2$ being larger than $\sigma^{2^*} + \sigma_b^{2^*}$. This seems to be the case around 5 and 10 km, and for most cases at 17.5 km (lowest three rows of figure 4.2). So as a guideline these results suggests that the tropospheric part of $\mathbf{B}$ should be deflated such that least the diagonal of $\mathbf{HBH^T}$ is less than the diagonal of $\mathbf{HB^*H^T} + \mathbf{R^*}$. This can be examined more systematically by probing 4.1 with a series of $\mathbf{R}$ matrices closer to the $\tilde{\mathbf{R}} = \mathbf{R}$ case.

It is also safe to conclude, that for the chosen $\mathbf{B}$ all probed $\mathbf{R}$ matrices have too high diagonal values in the troposphere. In the stratosphere reasonably good estimates of refractivity error covariance

[1] A strict analysis could be done in the common eigenspace of $\tilde{\mathbf{R}}$ and $\mathbf{R}$. However, both the input covariances, and the Desroziers estimates contain many missing values, which makes it cumbersome (not impossible) to diagonalize equation 4.1, thus a simple analysis of just the diagonals is chosen for the present report

diagonals can be read from figure 4.2, individually for COSMIC-1 and Metop, by visual interpolation to the point where $\tilde{\mathbf{R}} = \mathbf{R}$. So, keeping in mind that all estimates depend on the ROM SAF $\mathbf{B}$ matrices, it can be said that under this condition the ECMWF operational $\mathbf{R}$ matrix (e.g. upper left plot of Figure 3.30) appears to be fairly close to optimal in the middle stratosphere, because the estimated $\tilde{R}$ is close to the assumed $\mathbf{R}$. The results in Figure 3.30 suggest a minor deflation of $\mathbf{R}$ above 40 km, especially for Metop.

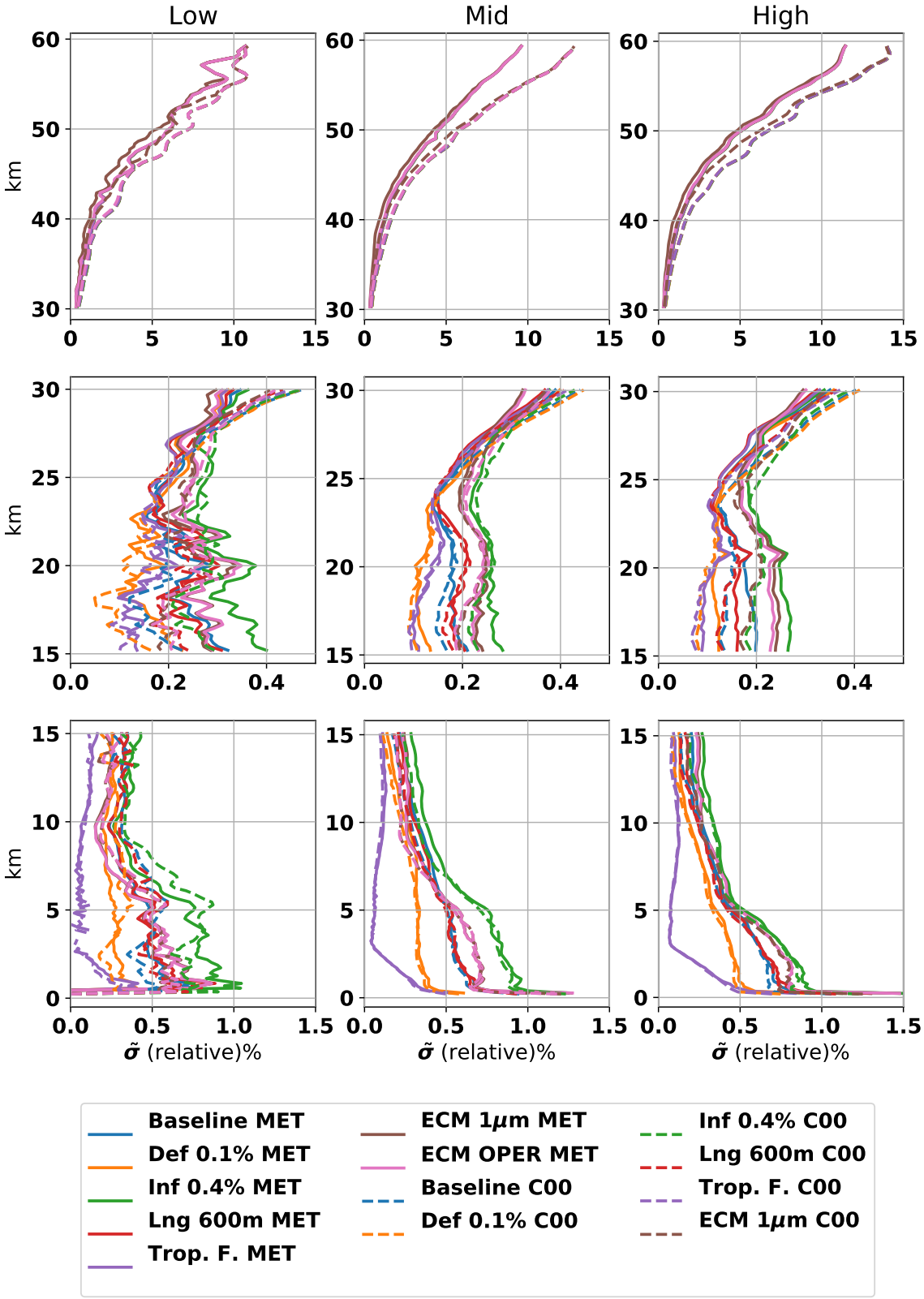


**Figure 4.1:** Diagnosed refractivity error standard deviations, i.e square root of diagonals of $\tilde{\mathbf{R}}$ matrices. Note the three different altitude ranges shown on the left axes, and the three different latitude bands; Low (0 to 30 deg.), Mid (30 to 60 deg.) and High (60 to 90 Deg)

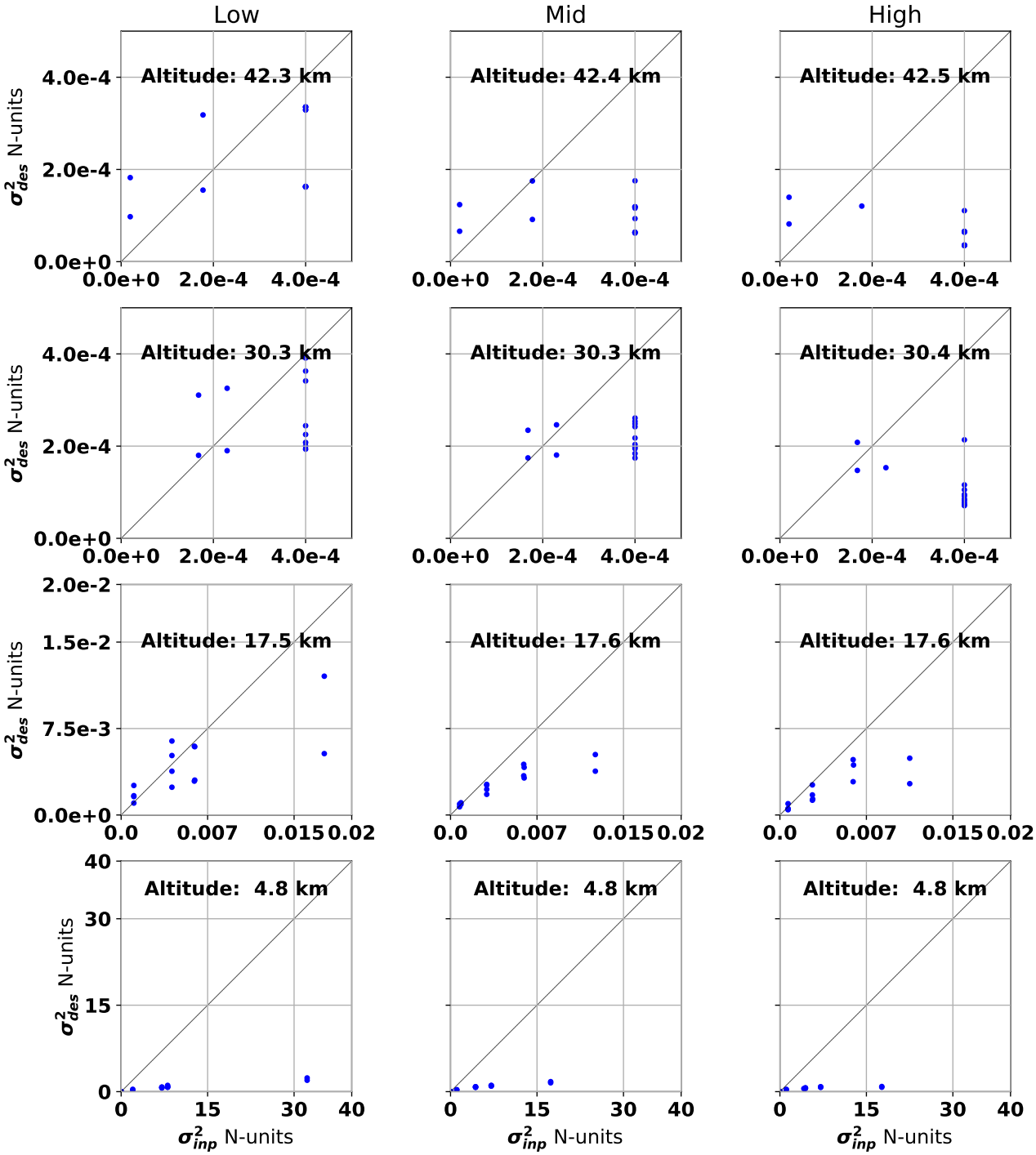


**Figure 4.2:** Diagnosed refractivity variances at 5 different height levels, and three different latitude bands: High (60 to 90 Deg), Mid (30 to 60 deg.) and Low (0 to 30 deg.). Note that while the Desroziers estimates (y-axes) are based on statistics from the whole latitude band in this plot, the input variance are representative matrix diagonal elements from single profiles. Blue dots; Metop and red dots; COSMIC-1. The diagonal lines mark where the diagnosed variance would equals the assumed variance.

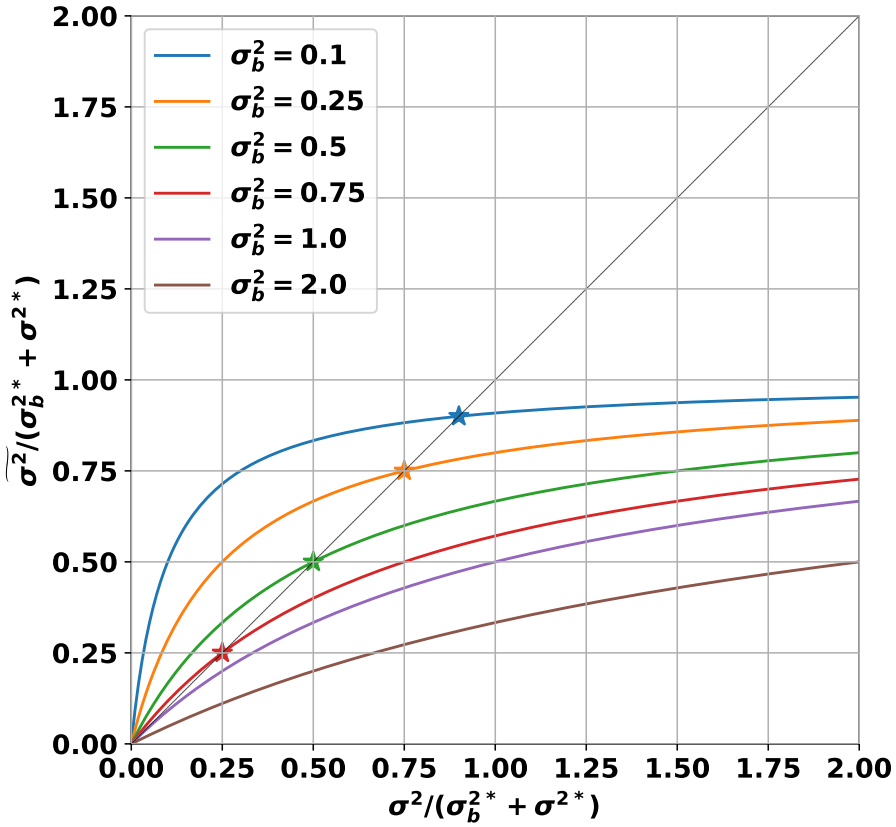


**Figure 4.3:** Diagnosed variance of a single level $\widetilde{\sigma^2}$, plottet as function of the assumed (input) variance $\sigma^2$. Both axes have been normalized with the directly observable quantity $1/(\sigma_b^{2*} + \sigma^{2*})$. The variances $\widetilde{\sigma^2}$, $\sigma^2$, $\sigma^{2*}$, $\sigma_b^2$ and $\sigma_b^{2*}$ correspond to the diagonal elements from $\tilde{\mathbf{R}}$, $\mathbf{R}$, $\mathbf{R}^*$, $\mathbf{HBH^T}$ and $\mathbf{HB^*H^T}$. The 7 curves correspond to different assumed values of $\sigma_b^2$, shown in the legend. The markers (*) are placed on the value of $\widetilde{\sigma^2} = \sigma^2$, which is only possible when $\sigma_b^2 < \sigma_b^{2*} + \sigma^{2*}$. Note that $\widetilde{\sigma^2} = \sigma^2$ only implies that $\sigma^2$ is true when also the assumed $\sigma_b^2$ equals the true $\sigma_b^{2*}$.

# 5 Conclusions and Outlook

1D-Var experiments have been performed with various choices of refractivity error covariance matrices. The experiments are listed at page 5. The results from the 7 1D-Var experiments may be summarized as follows.

In the Desroziers refractivity error covariance estimate produced by the **baseline** run, the standard deviation in the troposphere, at all latitudes for both Metop and COSMIC is much smaller than the assumed operational standard deviation. The lower and mid stratosphere refractivty errors are anticorrelated with the troposphere. These features persist for all experiments.

In the $\mathbf{R}$ **deflation** experiment the Desroziers matrix agrees very well with the assumed refractivity error covariance of 0.1% in the stratosphere, but in the troposphere the Desroziers matrix suggests an even smaller standard deviation. The biases of the baseline, i.e. negative humidity and temperature biases in the troposphere and positive temperature bias in the stratosphere, are enhanced by the deflation of refractivity error covariance.

In the **inflation** experiment the resulting Desroziers matrices are not just following the "suggested" standard deviation of $\mathbf{R}$ (0.4%). At mid and high latitudes, the Desroziers standard deviation in the stratosphere remains more or less on the same magnitude as in the background operational $\mathbf{R}$.

The **reduced correlation length** experiment Desroziers covariance still has a lower standard deviation than the baseline $\mathbf{R}$ at all altitudes, and at the same time the correlations have been slightly condensed around the diagonal, compared to the baseline Desroziers matrix. It is remarkable that the extra-tropical stratospheric temperatures, are allowed to depart considerably from the background in the reduced correlation length run, bringing them closer to GRUAN temperatures, and it is noteworthy that a solely reduction of refractivity error correlation length allows the specific humidity to become even more negatively biased than in the baseline run.

In the **tropospheric focus** run, with its extremely low tropospheric standard deviation assumption, the Desroziers method suggests an even lower standard deviation. Generally the baseline biases are enhanced as one would expect when combining the deflation of $\mathbf{R}$ with reduced correlation length, but at mid and high latitudes a remarkably strong dry bias of 10-15% is emerging, especially at mid latitudes between 6 and 10 km. The tropospheric focus experiment summarizes in which direction the radio occultation measurements point, if the background constraints are relaxed.

With the **in 3 $\mu$rad** The ECMWF error covariance allows RO to have a relatively strong impact at high altitude. Due to a less correlated $\mathbf{R}$, the ECMWF allows more impact in upper troposphere at midlatitudes than the ROM SAF does. In this case the diagonals of the Desroziers estimated $\tilde{\mathbf{R}}$ matrices are in good agreement with the input $\mathbf{R}$ in the stratosphere, though a little on the conservative side between 20 and 30 km. In the troposphere the Desrozier estimates are much lower that the assumed refractivity uncertainty like in all the other experiments.

With the **in 1 $\mu$rad** ECMWF refractivity error covariance matrix, the 1D-Var temperatures become strongly cold biased around 40 km, and at the same time the Desroziers matrices are stronger correlated at that altitude.

The ROM SAF operational refractivity covariance is too conservative at all levels both in terms of too high standard deviation and too broad correlation, given the current $\mathbf{B}$ matrix. For the chosen $\mathbf{B}$ all probed $\mathbf{R}$ matrices have too high diagonal values in the troposphere. Analysis of the **sensitivity of Desroziers estimates** to choice of $\mathbf{R}$ matrices leads to the conclusion that not only the refractivity

error covariance but also the background error covariance should be deflated in the troposphere.

The results obtained in this report will be used as guidelines in the definition of an $\mathbf{R}$ and $\mathbf{B}$ matrices for the ROM SAF second reprocessing. They will be viewed in combination with other results, including triple profile collocation analysis.

## Acknowledgements

Thanks to Sean Healy for provision of ECMWF error covariance matrices.

# Bibliography


[1] Desroziers, G., Berre, L., Chapnik, B., and Poli, P., Diagnosis of observation, background and analysis-error statistics in observation space, *Quarterly Journal of the Royal Meteorological Society*, *131*, 3385–3396, URL http://dx.doi.org/10.1256/qj.05.108, 2005.

[2] Dirksen, R. J., Sommer, M., Immler, F. J., Hurst, D. F., Kivi, R., and Vömel, H., Reference quality upper-air measurements: GRUAN data processing for the Vaisala RS92 radiosonde, *Atmospheric Measurement Techniques*, *7*, 4463–4490, URL https://www.atmos-meas-tech.net/7/4463/2014/, 2014.

[3] EUMETSAT, CDOP-3 cooperation agreement: Agreement between EUMETSAT and DMI on the third continuous development and operations phase (CDOP-3) of the radio occultation meteorology satellite applications facility (ROM SAF), ref.EUM/C/85/16/DOC/19, approved by the EUMETSAT council and signed at its 86th meeting on 7 December 2016., 2016.

[4] Eyre, J. R., On systematic errors in satellite sounding products and their climatological mean values, *Quart. J. Roy. Meteorol. Soc.*, *113*, 279–292, 1987.

[5] Healy, S., Estimates of GNSS radio occultation bending angle and refractivity error statistics, ROM SAF Report 26, ECMWF, 2016.

[6] Kursinski, E. R., Hajj, G. A., Schofield, J. T., Linfield, R. P., and Hardy, K. R., Observing earth's atmosphere with radio occultation measurements using the Global Positioning System, *J. Geophys. Res.*, *102*, 23.429–23.465, 1997.

[7] Kursinski, E. R., Healy, S. B., and Romans, L. J., Initial results of combining GPS occultations with ECMWF global analyses within a 1DVar framework, *Earth Planets Space*, *52*, 885–892, 2000.

[8] ROM SAF, Algorithm Theoretical Baseline Document: Level 2B and 2C 1D-Var products, SAF/ROM/DMI/ALG/1DV/002, a.

[9] ROM SAF, Algorithm Theoretical Baseline Document: Level 3 Gridded Data, SAF/ROM-/DMI/ALG/GRD/001, b.

[10] ROM SAF, Validation Report: Reprocessed Level 1B bending angle, Level 2A refractivity, Level 2A dry temperature CDR v1.0 products, SAF/ROM/DMI/REP/ATM/001, c.

[11] Scherllin-Pirscher, B., Steiner, A. K., Kirchengast, G., Kuo, Y.-H., and Foelsche, U., Empirical analysis and modeling of errors of atmospheric profiles from gps radio occultation, *Atmospheric Measurement Techniques*, *4*, 1875–1890, URL http://www.atmos-meas-tech.net/4/1875/2011/, 2011.

**ROM SAF (and earlier GRAS SAF) Reports**

| | |
|---|---|
| SAF/GRAS/METO/REP/GSR/001 | Mono-dimensional thinning for GPS Radio Occulation |
| SAF/GRAS/METO/REP/GSR/002 | Geodesy calculations in ROPP |
| SAF/GRAS/METO/REP/GSR/003 | ROPP minimiser - minROPP |
| SAF/GRAS/METO/REP/GSR/004 | Error function calculation in ROPP |
| SAF/GRAS/METO/REP/GSR/005 | Refractivity calculations in ROPP |
| SAF/GRAS/METO/REP/GSR/006 | Levenberg-Marquardt minimisation in ROPP |
| SAF/GRAS/METO/REP/GSR/007 | Abel integral calculations in ROPP |
| SAF/GRAS/METO/REP/GSR/008 | ROPP thinner algorithm |
| SAF/GRAS/METO/REP/GSR/009 | Refractivity coefficients used in the assimilation of GPS radio occultation measurements |
| SAF/GRAS/METO/REP/GSR/010 | Latitudinal Binning and Area-Weighted Averaging of Irregularly Distributed Radio Occultation Data |
| SAF/GRAS/METO/REP/GSR/011 | ROPP 1dVar validation |
| SAF/GRAS/METO/REP/GSR/012 | Assimilation of Global Positioning System Radio Occultation Data in the ECMWF ERA-Interim Re-analysis |
| SAF/GRAS/METO/REP/GSR/013 | ROPP PP validation |
| SAF/ROM/METO/REP/RSR/014 | A review of the geodesy calculations in ROPP |
| SAF/ROM/METO/REP/RSR/015 | Improvements to the ROPP refractivity and bending angle operators |
| SAF/ROM/METO/REP/RSR/016 | Simplifying EGM96 undulation calculations in ROPP |
| SAF/ROM/METO/REP/RSR/017 | Simulation of L1 and L2 bending angles with a model ionosphere |
| SAF/ROM/METO/REP/RSR/018 | Single Frequency Radio Occultation Retrievals: Impact on Numerical Weather Prediction |
| SAF/ROM/METO/REP/RSR/019 | Implementation of the ROPP two-dimensional bending angle observation operator in an NWP system |
| SAF/ROM/METO/REP/RSR/020 | Interpolation artefact in ECMWF monthly standard deviation plots |
| SAF/ROM/METO/REP/RSR/021 | 5th ROM SAF User Workshop on Applications of GPS radio occultation measurements |
| SAF/ROM/METO/REP/RSR/022 | The use of the GPS radio occultation reflection flag for NWP applications |
| SAF/ROM/METO/REP/RSR/023 | Assessment of a potential reflection flag product |
| SAF/ROM/METO/REP/RSR/024 | The calculation of planetary boundary layer heights in ROPP |
| SAF/ROM/METO/REP/RSR/025 | Survey on user requirements for potential ionospheric products from EPS-SG radio occultation measurements |

**ROM SAF (and earlier GRAS SAF) Reports (cont.)**

| | |
|---|---|
| SAF/ROM/METO/REP/RSR/026 | Estimates of GNSS radio occultation bending angle and refractivity error statistics |
| SAF/ROM/METO/REP/RSR/027 | Recent forecast impact experiments with GPS radio occultation measurements |
| SAF/ROM/METO/REP/RSR/028 | Description of wave optics modelling in ROPP-9 and suggested improvements for ROPP-9.1 |
| SAF/ROM/METO/REP/RSR/029 | Testing reprocessed GPS radio occultation datasets in a reanalysis system |
| SAF/ROM/METO/REP/RSR/030 | A first look at the feasibility of assimilating single and dual frequency bending angles |
| SAF/ROM/METO/REP/RSR/031 | Sensitivity of some RO measurements to the shape of the ionospheric electron density profile |
| SAF/ROM/METO/REP/RSR/032 | An initial assessment of the quality of RO data from KOMPSAT-5 |
| SAF/ROM/METO/REP/RSR/033 | Some science changes in ROPP-9.1 |
| SAF/ROM/METO/REP/RSR/034 | An initial assessment of the quality of RO data from Metop-C |
| SAF/ROM/METO/REP/RSR/035 | An initial assessment of the quality of RO data from FY-3D |
| SAF/ROM/METO/REP/RSR/036 | An initial assessment of the quality of RO data from PAZ |
| SAF/ROM/METO/REP/RSR/037 | 6th ROM SAF User Workshop |
| SAF/ROM/METO/REP/RSR/038 | An initial assessment of the quality of RO data from COSMIC-2 |
| SAF/ROM/METO/REP/RSR/039 | Impacts of RO mission differences on trends in multi-mission data records |
| SAF/ROM/METO/REP/RSR/040 | Anomalous GRAS radio occultations |
| SAF/ROM/METO/REP/RSR/041 | Assessment of sensitivity of the ROM SAF 1D-Var solutions to various error c |

ROM SAF Reports are accessible via the ROM SAF website: http://www.romsaf.org